





## Article

# Adapting and Verifying the Liming Index for Enhanced Rock Weathering Minerals as an Alternative Liming Approach

Francisco S. M. Araujo <sup>1</sup>, Andrea G. M. Chacon <sup>1,2</sup>, Raphael F. Porto <sup>1,3</sup>, Jaime P. L. Cavalcante <sup>4</sup>, Yi Wai Chiang <sup>1</sup>  
and Rafael M. Santos <sup>1,\*</sup>

<sup>1</sup> School of Engineering, University of Guelph, Guelph, ON N1G 2W1, Canada; faraujo@uoguelph.ca (F.S.M.A.); monsalva@uoguelph.ca (A.G.M.C.); porto@eq.ufrj.br (R.F.P.); chiange@uoguelph.ca (Y.W.C.)

<sup>2</sup> Facultad de Ingenieria, Universidad de La Sabana, Chía 140013, Colombia

<sup>3</sup> Chemical Engineering, Federal University of Rio de Janeiro, Rio De Janeiro 21941-909, RJ, Brazil

<sup>4</sup> Department of Natural Sciences, Federal University of Pernambuco, Recife 50670-901, PE, Brazil; jaimephasquinell@gmail.com

\* Correspondence: santosr@uoguelph.ca

**Abstract:** Acidic soils limit plant nutrient availability, leading to deficiencies and reduced crop yields. Agricultural liming agents address these issues and are crucial for deploying silicate amendments used in enhanced rock weathering (ERW) for carbon sequestration and emission reduction. Grower recommendations for liming agents are based on the liming index (LI), which combines the neutralizing value (NV) and fineness rating (FR) to predict a mineral's acidity neutralization relative to pure calcite. However, the LI was originally developed for carbonate minerals, and its applicability to silicates remains uncertain, with studies often yielding inconclusive results on soil carbon and liming efficiency. This study aims to evaluate the liming efficiency of silicates. We determined the LI of five candidate ERW minerals (basalt, olivine, wollastonite, kimberlite, and montmorillonite) and compared them to pure calcite. Post-NV acid digestion, we characterized the minerals and soils, applying nonparametric statistical tests (Wilcoxon, Kendall) to correlate liming results with LI, dosage, and amendment methods. We developed an empirical model incorporating mineralogy and kinetics to explain silicate behavior in liming, considering soil, climate, and crop factors.

**Keywords:** liming; ERW; agricultural index; acid digestion; climate change; sustainable agriculture



**Citation:** Araujo, F.S.M.; Chacon, A.G.M.; Porto, R.F.; Cavalcante, J.P.L.; Chiang, Y.W.; Santos, R.M. Adapting and Verifying the Liming Index for Enhanced Rock Weathering Minerals as an Alternative Liming Approach. *Land* **2024**, *13*, 1839. <https://doi.org/10.3390/land13111839>

Academic Editors: Ioannis Charalampopoulos and Dionisios Gasparatos

Received: 30 September 2024

Revised: 28 October 2024

Accepted: 3 November 2024

Published: 5 November 2024



**Copyright:** © 2024 by the authors. Licensee MDPI, Basel, Switzerland. This article is an open access article distributed under the terms and conditions of the Creative Commons Attribution (CC BY) license (<https://creativecommons.org/licenses/by/4.0/>).

## 1. Introduction

The pH of the soil affects plant growth and nutrient availability. Plants have specific pH preferences for optimal growth, and the soil pH can influence the availability of various nutrients essential for plants. Soil acidity is a potentially serious land degradation issue. Soil acidification can affect agricultural productivity and sustainable farming [1]. It can penetrate subsoil layers, creating significant challenges for plant root growth and corrective measures. Several factors contribute to soil acidity. These include acidic precipitation, the deposition of acidifying gases or particles from the atmosphere, and the use of ammonium-based fertilizers, urea, and elemental sulfur fertilizers [2]. This study compares the liming efficiency of five silicate-based minerals (basalt, olivine, wollastonite, kimberlite, and montmorillonite) against that of calcite using liming index (LI), dosage, and amendment methods to develop an empirical model to better predict the liming effect on soil.

Liming studies are crucial for sustainable agricultural practices to mitigate soil acidity, enhance nutrient availability, and improve crop productivity [3–5]. Grower recommendations for liming agents, based on the liming index (LI), are pivotal. The LI, calculated from the neutralizing value (NV) and fineness rating (FR) of a mineral, predicts its acidity neutralization efficiency compared to pure calcite [6]. Although LI was originally designed for carbonate minerals, studies on silicate-based minerals are scarce. Information on LI or silicate amendments is often lacking, and existing studies on silicate liming have frequently

produced inconclusive results regarding its impact on liming and soil carbon [7–11]. Silicate liming may even cause a short-term decline in soil organic carbon, similar to conventional liming practices [12]. These findings underscore the need for careful consideration of amendment approaches to optimize agronomic benefits and soil carbon storage.

Within the five research focuses, a number of liming processes have been investigated and can be classified as follows: (1) the benefits of liming on soil structure and plant growth in no-till cropping systems and acid soils [13]; (2) acid soil tolerance in plants and the long-term impacts of liming [14]; (3) soil and crop response to wood ash and lime application [15]; (4) aggregate stability in low-input acid soils [16]; (5) impacts of lime and phosphogypsum in tropical soils under no-till conditions [17].

This study focused on investigating how the use of silicates as liming agents impacts soil acidity and soil organic carbon content. Similar studies are related to those of Doe et al. [18] reviewed the use of silicates as soil amendments, and Brown et al. [19] evaluated the effectiveness of silicate-based materials in ameliorating acidic soils. Martinez et al. [20] explored how silicates can regulate soil pH and carbon sequestration, and Clark et al. [21] discussed the use of silicates as liming agents using field trials. However, none of these studies have progressed toward examining distortions in the neutralizing value (and LI) when calculating the liming effect of silicate minerals using laboratory and mesocosm data.

Additionally, this research aims to develop an empirical model that incorporates factors such as dissolution kinetics, the impact of pH changes on mineral dissolution rates, and the formation of secondary phases. Other researchers have previously employed this approach with notable success. In the study by Wilkin and Digiulio [22], it was observed that changes in pH and aqueous ion concentrations affect the dissolution rates of silicates, with slow dissolution rates compared to carbonate minerals. This highlights the importance of considering the kinetics of silicate dissolution in predictive models. Furthermore, the study by Bandyopadhyay et al. [23] discussed the effects of incorporating silicate layers on the crystallization kinetics of polymers, indicating the need to understand how mineralogy influences reaction rates. The incorporation of mineralogical data into predictive models is crucial, as shown in the study by Kittridge [24], where the influence of mineralogy on the velocity of carbonate rocks was investigated. Therefore, understanding how mineral composition affects physical properties can provide valuable insights into the behavior of silicates during liming processes. Overall, to develop an empirical model for predicting the liming behavior of silicates, it is essential to consider the kinetics of silicate dissolution, the influence of pH changes on reaction rates, and the role of mineralogy in determining the final mineral phases formed. By integrating these factors into a comprehensive model, it is possible to improve predictions of the liming behavior of silicates.

To address these questions, we undertook a multifaceted approach to examine the properties and behavior of silicate minerals through the following steps:

- The neutralization value (NV) and liming index (LI) of the minerals were calculated using two acid digestion methods to assess their reactivity with acidic components.
- Investigate the mineral behavior during NV reactions using electron microscopy and X-ray diffraction to elucidate the underlying mechanisms.
- Conduct a series of liming tests in a controlled greenhouse environment with varying initial soil acidities and mineral dosages over several weeks.
- Relationship between liming outcomes from mesocosm experiments and previously determined LI values in the laboratory.

Finally, the results of these liming tests and their correlation with the LI are presented in this study, providing valuable data for developing a preliminary empirical model that is more suitable for predicting the liming effectiveness of silicates. By developing a more suitable empirical model for predicting the liming effectiveness of silicates, farmers can achieve more precise soil management, leading to improved crop cost efficiency, environmental sustainability, and long-term soil health [25–27]. This advancement empowers farmers to use better tools to make informed decisions, ultimately enhancing their productivity and sustainability.

## 2. Materials and Methods

### 2.1. Liming Index, Fineness Rating, and Neutralizing Value

The liming index (LI) refers to the capacity of a mineral to neutralize soil acidity and increase the pH of the soil. This index is a crucial factor in determining the effectiveness of different minerals in correcting soil acidity, which in turn affects nutrient availability and overall plant health [28]. Minerals with alkaline properties, such as calcium carbonate (limestone or dolomite), can be applied to soil to increase its pH and alleviate its acidity. The LI plays a crucial role in deciding which minerals to use as soil amendments, as it helps determine how much of a material is required to achieve the desired soil pH. The neutralizing value (NV) is the amount of acid that a given quantity of limestone neutralizes when it is dissolved. It is expressed as a percentage of the NV of pure calcium carbonate. A limestone that will neutralize 90% is said to have an NV of 90.

Another factor that affects the value of limestone as a neutralizer of acidity is the fineness rating. A limestone's fineness rating is a measure of its particle size distribution and is determined using sieves. Smaller particles with larger surface areas will rapidly change the pH of the surrounding soil. Particles with a diameter of 250 µm or less are said to be 100% effective [28]. However, for some applications, a combination of particle sizes is desirable to provide the soil with both short-term and long-term changes in soil pH [29]. The LI combines the (NV) and fineness rating (FR) of limestone, offering a means to contrast various sources of limestone. Limestone with an elevated LI necessitates a reduced application rate compared to limestone with a lower LI. The LI of a limestone is calculated using the following formula:

$$LI = \frac{NV \times FR}{100} \quad (1)$$

NV is typically expressed as the percentage of calcium carbonate equivalent (CCE), which represents the fraction of the mineral's weight that is equivalent to that of pure calcium carbonate ( $\text{CaCO}_3$ ). In this research, the neutralizing value was determined by 2 (two) methods, namely, methods "A" and "B". In method "A", according to ISO 20978:2020 [11], 0.5 g of a sample was treated in a 250 mL beaker with 50 mL of 0.5 N hydrochloric acid by heating for 10 min. Later, the sample was potentiometrically titrated with 0.25 N sodium hydroxide until the pH reached 7.0 and held for 1 min. The neutralizing value was estimated as follows (2):

$$NV = \frac{(c \times (M_1 \times V_1 \times f_1 \times A - M_2 \times V_2 \times f_2)) \times 100}{m_t \times A} \quad (2)$$

where NV is the neutralization value (%),  $c$  is 0.050 when NV is expressed as  $\text{CaCO}_3$ ,  $M_1$  is the molarity of HCl (mol/L),  $V_1$  is the volume of HCl (mL),  $M_2$  is the molarity of NaOH (mol/L),  $V_2$  is the volume of NaOH (mL),  $m_t$  is the sample weight (g), and  $A$  is equal to 1 for method "A" and 0.5 for method "B", as classified in the ISO 20978:2020 [11]. The correction factors  $f_1$  and  $f_2$  may be omitted if the molarity values are actual rather than theoretical.

Method "B" was employed to eliminate iron interference in certain liming minerals by utilizing a hydrogen peroxide solution to oxidize any reduced iron present. Ferrous ions from silicate liming materials can oxidize and consume  $\text{OH}^-$  from the alkaline solution used during titration. Hydrogen peroxide reacts with iron ions before titration and forms ferric and ferrous ions in a neutral reaction. In method "B", 0.5 g of the sample was prepared and placed into a 250 mL Erlenmeyer flask. The inner surfaces of the Erlenmeyer flasks were rinsed with approximately 10 mL of distilled water. Subsequently, 30 mL of 0.5 mol/L HCl solution was added to the flask with continuous stirring. The solution was heated for approximately 10 min to dissolve the sample with the assistance of a magnetic stirrer. After sample dissolution, the solution was allowed to return to room temperature, and then 100 mL of water was added, followed by the addition of 5 mL of hydrogen peroxide solution. The solution was quantitatively transferred to a 200 mL graduated flask,

and water was added to make up the volume of the graduated flask and homogenize the solution.

The resulting solution was filtered through a dry filter and a beaker to collect the filtered solution. The initial portion was discarded. An aliquot of 100 mL of the filtered solution was pipetted into a 250 mL beaker. Subsequently, titration was performed using a 0.25 mol/L NaCl solution with a pH meter and a stirrer until a pH of 4.8 was attained, and the solution was stabilized for 1 min.

## 2.2. Pot Experiment Description and Design

Liming material samples were obtained from manufacturers in Canada and the United Kingdom. Wollastonite was obtained from Canadian Wollastonite Inc. (Seeley's Bay, ON, Canada); bentonite from Absorbent Products Ltd. (Kamloops, BC, Canada); basalt from Rock Power Solutions Inc. (Woodstock, ON, Canada); olivine from GreenSand Group (Enkhuizen, Netherlands); kimberlite from DeBeers Group (Attawapiskat, ON, Canada); and CaCO<sub>3</sub> from Fisher Scientific (Hampton, NH, USA). All minerals were ground and sieved at 250 microns to obtain the desired fineness. The soil/mineral dosage was considered to have values of 1.2, 1, 0.8, and 0.6 (rate 1, rate 2, rate 3, and rate 4), where the optimal amount of mineral was equal to 1. This value was calculated considering the LI and the commercial application of each mineral [30].

To replicate the conditions that will occur in a crop field, 2 (two) application methods were used: mixing the mineral with the soil ("mixed") (up to 15 cm to the top of the soil) and applying the mineral entirely on the surface ("surface application"). The experimental pots were set up on a building rooftop at the University of Guelph (Guelph, ON, Canada). The first soil was organic-rich soil labeled commercial garden club black earth topsoil without fertilizer. To ensure its acidity, it was mixed with organic matter (peat moss) at a 7:3 ratio. The final pH of the soil/peat moss mixture ranged from 5.9 to 6.1. Pots of 6.724 m<sup>2</sup> were filled with 150 g of soil/peat moss. Naturally acidic (pH < 6.0) mineral-rich soil used for agricultural purposes was collected from a crop field at the intersection of Jones Baseline and Hwy 7, close to the city of Guelph, ON, Canada (N 43.590609, W -80.195794).

No mineral fertilizers were added. The same amount of mineral was used for both mineral applications. To simulate the conditions that will occur in a crop field, the amount of irrigation (50 mL) was determined considering the annual precipitation of the local region (Guelph, ON, Canada), where the experiment was conducted from irrigation volume by province report [31]. The water was acidified with HCl to obtain a pH between 5 and 5.5 (the pH of rainwater).

In the first experiment, 48 pots were used, divided among six mineral types (bentonite, basalt, wollastonite, kimberlite, olivine, and calcium carbonate), four soil-to-mineral ratios (ratio 1 to ratio 4), and two methods of mineral application (mixed and surface application). Additionally, two soil control pots were included to observe the pH behavior of the soil without any mineral additions, resulting in a total of 50 pots for the experiment. The second experiment followed the same design, using 48 pots divided among the six mineral types, the four soil-to-mineral ratios, and the two methods of mineral application. Again, two soil control pots were included, resulting in a total of 50 pots for the experiment. Figure 1 represents the design of the experiment.

## 2.3. pH Measurement

A soil pH meter (Bluelab Soil pH pen) was calibrated with buffered solutions (pH 4.0, 7.0, and 10) prior to each sampling. To measure the pH of each pot, the storage cap was removed. This was conducted by unscrewing the cap and pulling it to remove the probe. The pen was turned on, and the probe was inserted into the pot. The pen was removed after the pH reading stabilized on the display. The soil was rinsed after use to remove any nutrient or soil deposits before the next measurement. For all the samples, three pH measurements were taken in different parts of each pot. The simple average was recorded. The pH was measured after watering. As indicated by Zarate-Valdez et al. [32], soil pH is

directly influenced by changes in moisture content. Then, to minimize variations, the pots were watered, and the pH values were measured immediately afterward. Temperature and humidity ambient readings were also recorded using greenhouse sensors. These activities were consistently performed at the same time each day throughout the experiment.

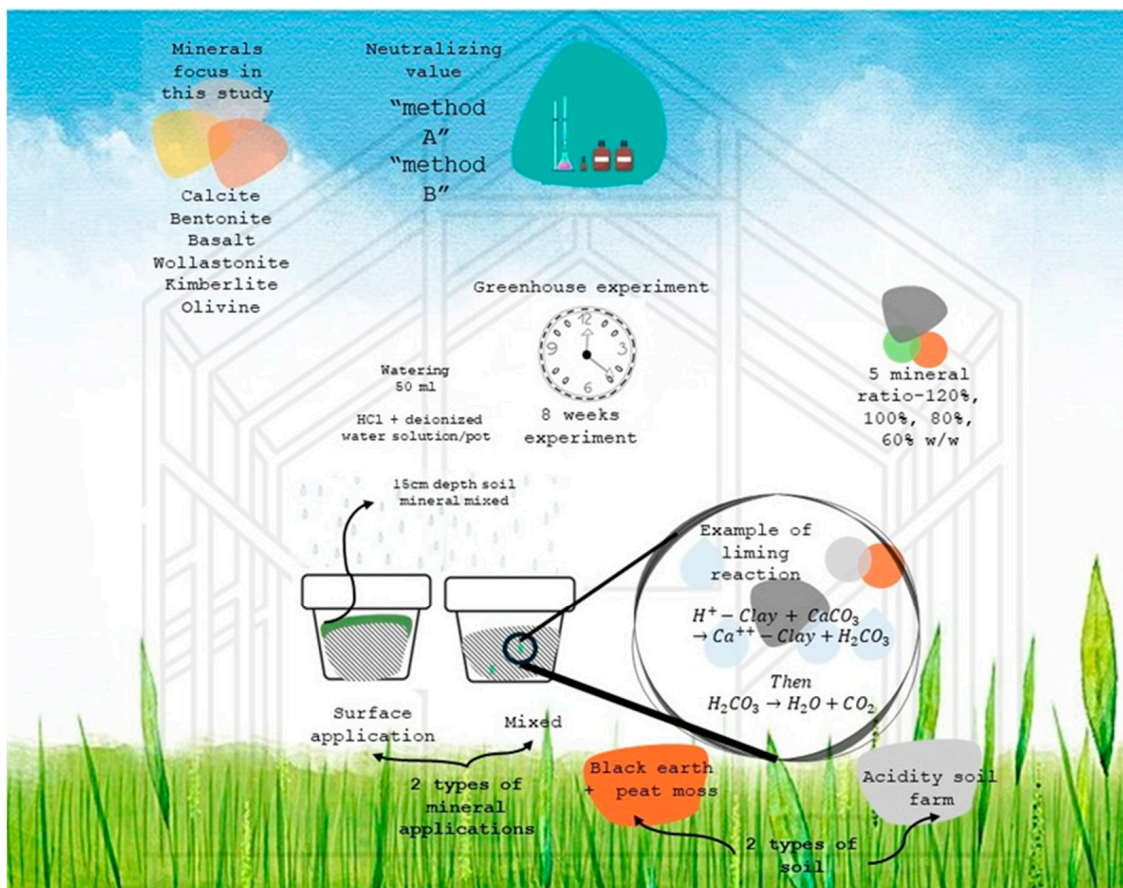


**Figure 1.** Experimental design outlining key parameters, including the types of minerals used, liming measurement methods, mineral application techniques, mineral-to-soil ratios, and duration of the experiment.

These measurements were taken two days a week over a period of 7 weeks. At the beginning and end of the experiment, samples from each pot were taken to the laboratory to be measured with a standard bench pH meter (PH 2700 Benchtop pH Meter, Oakton, Charleston, SC, USA) following the standard ASTM D4972 [33]. Both results obtained were compared for better accuracy.

#### 2.4. Analysis Criteria

As soil is a complex and heterogeneous medium, this dynamic system (composed of minerals, organic solids, and aqueous and gaseous components) is subject to short-term changes in moisture content, pH, and redox conditions [34]. Soil pH is a critical factor that influences the chemical behavior of minerals and various processes within the soil. However, this feature is inherently variable. Many recent works attributed these variations to the complex interactions between environmental and anthropogenic factors, such as land use changes, soil management practices, and environmental conditions [35], as well as soil buffering capacity [36]. To address pH heterogeneity in soils, several statistical techniques have been used with relative success, such as hierarchical cluster analysis (HCA), principal component analysis (PCA) [37–40], classification [41], and regression [42].

In the present study, statistical techniques were employed to investigate soil pH behavior, considering six types of minerals in their respective experiments (soil type and

application method). Initially, the aim was to assess whether the selected minerals exhibited a liming effect by altering the soil pH relative to the soil buffer pH (h1) and a reference mineral ( $\text{CaCO}_3$ ) (h2). For this purpose, the nonparametric Wilcoxon test was used with relative success (Equation (3)). Additionally, to evaluate the trend of increasing pH over time—indicating the occurrence of liming—the data were smoothed using the simple moving average (SMA) technique (Equation (4)). This smoothing procedure is justified because the natural variability of pH values made it difficult to identify trends in the raw data. By smoothing this variability, the trend became more discernible. Once smoothed, the pH data were subjected to Kendall's correlation test to verify the significance of the observed trend in the SMA and the degree of correlation between pH values and time. This test is recommended for evaluating trends in time-related data, providing a correlation coefficient known as Kendall's Tau ( $\tau$ ) (Equation (5)).

$$\begin{aligned} (Z = [X_1, X_2, \dots, X_m, Y_1, Y_2, \dots, Y_n]); \\ (Z_{rank} = [1, 2, \dots, m + n]); \\ U_1 = n_1 n_2 + \frac{n_2(n_2+1)}{2} - R_2; U_2 = n_1 n_2 + \frac{n_1(n_1+1)}{2} - R_1 \end{aligned} \quad (3)$$

where  $X$  and  $Y$  are groups of samples,  $Z_{rank}$  is a smaller set of  $X$  and  $Y$  combined, and  $U$  is a U test statistic

$$SMA_t = \frac{1}{n_{sma}} * (x_t + x_{t-1} + x_{t-2} + \dots + x_{t-(n_{sma}-1)}) \quad (4)$$

where  $x_t$  represents the time series in period  $t$ , and  $n_{sma}$  determines the number of previous periods considered in the simple moving average (SMA)

$$\tau = 1 - \frac{2(\text{number of discordant pairs})}{\frac{n(n-1)}{2}} \quad (5)$$

Finally, the percentage rate of pH change was calculated throughout the experiment for each pot. Experiments with a low variation rate were considered more consistent regarding the liming effect. Using these values, we filtered the best candidates meeting the following three criteria simultaneously: (i) statistically significant pots with a  $p$ -value  $< 5\%$  in the Wilcoxon test, (ii) statistically significant pots for trend presence with a  $p$ -value  $< 5\%$  in the Kendall test and higher Tau ( $\tau$ ) values, indicating significant trends and a high correlation between pH and time, and (iii) pots with the lowest variation rate.

## 2.5. Empirical Model

The empirical model is based on the weathering rate of the most reactive mineral in each sample considering its degree of purity, standardized chemical formula, and particle size distribution (PSD). Since the liming response occurs over a short period, it is not the entire rock that reacts but rather its most reactive phase. The modeling focused on these most reactive phases of each mineral to calculate the weathering rates ( $Wr$ ). For instance, ankerite was selected for kimberlite, fosterite for olivine, and anorthite for basalt.

We utilized the weathering rates for our alkaline minerals based on the data provided by Palandri and Kharaka [43]. First, the logarithm of the Arrhenius pre-exponential factor at  $25^\circ\text{C}$  ( $298.15\text{ K}$ ) ( $\log A$ ,  $\text{mol}\cdot\text{m}^{-2}\cdot\text{s}^{-1}$ ) was calculated using Equation (6). Then, the weathering rate was determined using Equation (7) as a function of pH and temperature ( $25^\circ\text{C}$ ). We used the equation coefficients  $k$ ,  $E$ , and  $n$  for the neutral pH range ( $\sim 6-9$ ), as reported by Palandri and Kharaka [43], taking into consideration the recommendations of Haque et al. [44] on selecting an appropriate weathering mechanism for slightly acidic conditions that lie in between the acidic and neutral mechanisms. Here,  $k$  is the calculated rate constant at  $25^\circ\text{C}$  and  $\text{pH} = 0$  ( $\text{mol}\cdot\text{m}^{-2}\cdot\text{s}^{-1}$ ),  $E$  is the Arrhenius activation energy ( $\text{kJ}\cdot\text{mol}^{-1}$ ), and  $n_{\text{H}^+}$  is the reaction order with respect to  $\text{H}^+$ .

$$\log A = \log K + \frac{E \times 1000}{2.3025 \times 8.314 \times 298.15} \quad (6)$$

$$\log W_r = \log A - \frac{E \times 1000}{2.3025 \times 8.314 \times T} - n_{H^+} \times pH \quad (7)$$

The equation for the empirical model is given for (8):

$$\text{Empirical model} = \log \left( \frac{SSA}{M \times \%purity} \times W_r \right) \quad (8)$$

The model focused on the weathering rate of the most reactive mineral phase, rather than the mineral as a whole. This approach is logical if we consider liming as a rapid event that does not allow the entire rock to react fully. Consequently, each mineral phase was identified using X-ray diffraction (XRD) and quantified with PROFEX software v5.4.0. The diffractometer (Malvern Panalytical Empyrean) operated with Cu K $\alpha$  radiation at 45 kV and 40 mA, and the diffraction patterns were collected over a 2 $\theta$  range of 20–50° at a scan rate of 1°/min. This analysis provided insights into the purity of each mineral phase. The empirical model then incorporated these purity measurements into the formula.

The molar mass M (g/mol) of the standard chemical formula was calculated using the elemental composition, expressed as oxides, and determined by wavelength dispersive X-ray fluorescence (WDXRF).

The particle size distribution (PSD) was measured by sieving and sedimentation. The specific surface area (SSA) in m<sup>2</sup>/g was measured using a physisorption analyzer (BET) and laser diffraction analysis (Malvern Mastersized SM). The SSA of minerals is usually measured via a Brunauer–Emmett–Teller (BET) analysis of volumetric nitrogen adsorption isotherms. However, this technique has accuracy limitations for materials <0.5 m<sup>2</sup>/g, requires dry samples, must be measured at 77 K and has slow sample preparation times (drying/degassing).

A good alternative method for determining the SSA is laser diffraction or low-angle laser light scattering (LALLS), which can easily determine the SSA by using a laser as a source of light and a photosensitive detector. The particles in suspension can be measured by recirculating the sample in front of the laser beam. This method has become the preferred standard for characterization and quality control in many industries. This method relies on the fact that the diffraction angle is inversely proportional to the particle size. The advantages of this method include the following: (1) no need to calibrate against a standard, (2) it has a wide dynamic range according to ISO 13320:2020 [45] (0.1 to 3000  $\mu$ m), (3) it can measure dry powders directly in conjunction with suspension analysis, (4) the entire sample, instead of some part of it is measured through the laser beam, (5) the volume distribution is generated directly, which is equal to the weight distribution if the density is constant, and (6) the method is rapid, highly repeatable and has high sensitivity to multi-modal distributions. In this work, we refer to the specific surface area (SSA) measured by the BET method as the BSSA. Conversely, the SSA measured by laser diffraction will be termed GSSA, where “G” stands for geometrical, reflecting that this measurement is based on the geometry of the particle rather than the pore structure, as in the BET method.

## 2.6. Ranking

Due to our hypothesis that the NV would not effectively predict the liming of silicate minerals, we formulated an empirical model considering mineralogy and reaction kinetics to explain the material behavior. This model considers weathering rates, specific surface area, mean molecular mass, and the purity of the more reactive phase of the rock (see item 2.6).

To assess the model’s reliability, we opted to compare its outcomes with those of NV in a ranked format (9):

$$\text{Rank}_i = \min \left( \alpha * \sum \left| \text{Rank} \left( S_{pH_i} \right) - \text{Rank} \left( EM_i \right) \right|, \gamma * \sum \left| \text{Rank} \left( S_{pH_i} \right) - \text{Rank} \left( NV_i \right) \right| \right) \quad (9)$$

where

- $\text{Rank}_i$  : The final ranking for the  $i$ -th experiment.

- $Rank(S_{pH_i})$  : Ranking of the slope of the pH curve for the  $i$ -th experiment.
- $Rank(EM_i)$ : Ranking of the empirical model for the  $i$ -th experiment.
- $Rank(NV_i)$ : The ranking of the NV indicators for the  $i$ -th experiment.
- $\alpha$ : The weight assigned to the difference between the rankings of the slope of the pH curve and the empirical model.
- $\gamma$ : The weight assigned to the difference between the rankings of the slope of the pH curve and the NV indicator.
- min: The minimum function, which selects the smaller value between two terms.

Equation (9) is a ranking formula used to assess the performance of different experiments based on three factors: the slope of the pH curve, an empirical model, and an indicator NV. The formula consists of two terms:

1. The first term ( $\alpha * \Sigma |Rank(S_{pH_i}) - Rank(EM_i)|$ ) calculates the difference in ranking between the slope of the pH curve and the empirical model, multiplied by a weight factor  $\alpha$ . This term assesses how well the empirical model correlates with the experimental data defined here by the slope of the pH curve.
2. The second term ( $\gamma * \Sigma |Rank(S_{pH_i}) - Rank(NV_i)|$ ) calculates the difference in ranking between the NV and the slope of the pH curve, multiplied by a weight factor  $\gamma$ . This term assesses how well the NV correlates with the slope of the pH curve.

The overall ranking ( $Rank_i$ ) for each experiment is then determined by the minimum value between the two terms. This means that the experiment's ranking is based on the factor (slope vs. empirical model or slope vs. NV indicator) that shows the least discrepancy. Lower values of ( $Rank_i$ ) indicate a better correlation between the pH curve slope and either the empirical model or the NV indicator, depending on which factor has a smaller discrepancy.

### 3. Results

#### 3.1. Neutralizing Value

As mentioned in the previous section, the first step involves calculating the liming index (LI) or agricultural index and, consequently, the neutralizing value of the selected mineral samples using two acid digestion methods. The goal is to determine whether the LI accurately reflects the liming behavior of silicate-based minerals and to provide justifications for the varying values observed.

Table 1 shows the mean neutralization values (NVs) obtained for various minerals in the study. Significantly, calcium carbonate demonstrated the highest NV at 103.16%, which is consistent with its reference status in this analysis [11].

Olivine had the second-highest NV value for Method A in Table 1. Olivine is a family of nesosilicate minerals primarily composed of magnesium and iron silicates, and tends to dissolve more slowly than carbonates. However, certain components detected through XRD in the olivine sample (see Section 3.1.1), such as forsterite, lizardite, and clinocllore, are likely to contribute partially to the neutralization of soil acidity, releasing magnesium ions during weathering [46–49]. The notable 14.92% variance between the NV analysis results via methods A (59.33% eq  $CaCO_3$ ) and B (74.25% eq  $CaCO_3$ ) indicates the presence of substantial ferrous iron in the olivine sample (likely in the fayalite in solid solution with forsterite), influencing the obtained NV. An important caveat is that high concentrations of nickel ions in olivine may restrict its use for agricultural purposes [50].

The NV results for the two sources of kimberlite samples are presented in Table 1, and this mineral ranks third among those tested in terms of highest NV. Kimberlite sample 2 displayed the higher of the two NV values with Method A. XRD analysis (see Section 3.1.1.) highlights carbonates as the significant contributors to the NV of this mineral. Additionally, magnesium silicate minerals such as lizardite, chrysotile, and forsterite can make a relatively smaller yet significant contribution to soil acidity neutralization. Method B yielded a notable 10.44% difference, indicating iron interference in the NV analysis, likely attributable to ankerite.



**Table 1.** Neutralizing values (NV) of various minerals analyzed using two methods. This table presents the NV of different minerals, expressed as a percentage equivalent to calcium carbonate (% eq CaCO<sub>3</sub>) and calcium oxide (% eq CaO), as determined by Method A and Method B. Data are provided for each mineral where applicable.

Mineral	NV Method A		NV Method B	
	(% eq CaCO <sub>3</sub> )	(% eq CaO)	(% eq CaCO <sub>3</sub> )	(% eq CaO)
Bentonite	2.510	1.400	-	-
Basalt	13.14	7.360	25.63	14.35
Coarse wollastonite 1	14.72	8.240	-	-
Coarse wollastonite 2	18.57	10.40	-	-
Ground wollastonite	19.85	11.11	20.82	11.66
Kimberlite 1	40.68	22.78	-	-
Kimberlite 2	51.25	28.70	61.89	34.66
Olivine	59.33	33.23	74.25	41.58
Oyster shell	98.29	55.04	-	-
Calcium carbonate	103.16	57.77	-	-

The wollastonite sample had an NV of only 19.85% eq CaCO<sub>3</sub>. XRD and SEM analyses (see Section 3.1.1) indicated that diopside and wollastonite should be the main contributors to the attained NVs [51], but the NV values suggest incongruent or incomplete reactivity. It would have been expected for wollastonite to have a larger NV value than kimberlite based on our previous research in Chai et al. [52]. In that study, we assessed the reactivity and CO<sub>2</sub> uptake capacity of kimberlite and wollastonite through carbonation. The study concluded that wollastonite, which is rich in fast-weathering calcium silicate, is more reactive than kimberlite, which contains slow-weathering hydrated magnesium silicate and aluminosilicates. But in a carbonation study, the innate carbonate content of the mineral does not positively count towards the evaluation of reactivity, while it does in the case of liming and NV testing. Wollastonite also exhibited a lower NV value than olivine (Table 1). In our previous study, Santos et al. [53], on nickel extraction from olivine, which combined conventional acid leaching with a pretreatment step involving mineral carbonation, demonstrated that although olivine carbonation is relatively slow even under elevated temperature and pressure, it can achieve 100% carbonation without experiencing passivation issues. On the other hand, while wollastonite should theoretically be faster to weather than olivine, it appears to undergo more passivation or more incongruent dissolution during acid digestion, resulting in a lower NV value.

Passivation is the effect of coating the surface of the dissolving mineral with reaction byproducts, slowing the reaction process and reducing the total extent of carbonation [54]. Passivation, as a linkage between silicate dissolution and secondary precipitation affecting carbonation, is one of the questions addressed by recent investigators [49,55–60]. It has been proposed that the formation of an amorphous silica layer could act as a passivation coating, which could partly inhibit further dissolution of silicate (e.g., Béarat et al. [61], Huijgen et al. [51], and Kashim et al. [62]), but the formation of secondary minerals can also play this role (more on this in Section 3.1.1.). Additionally, for olivine, the passivation hypothesis can also be related to the atomic ratios. Wollastonite has 1 Ca atom for every Si atom, whereas forsterite has 2 Mg atoms for every Si atom. This means that olivine has less Si to hinder the reaction, allowing it to react more extensively even if slower. These phenomena are in line with the accelerated carbonation tests reported by Huijgen et al. [51] and Chai et al. [52], wherein the maximal reaction extents reported were 70% and 55.7%, respectively. Therefore, a degree of passivation or incongruent dissolution is to be expected with wollastonite, even if it does theoretically weather faster. This also suggests that the NV test is being more predictive of the ultimate reactivity of wollastonite versus olivine, than its weathering rate.

Basalt, a volcanic igneous rock, varies in efficiency as a pH corrector based on its mineralogical composition and displays a lower NV in Table 1 (13.14% eq. CaCO<sub>3</sub>). XRD

analysis (see Section 3.1.1) revealed a varied combination of plagioclase, chlorite, pyroxene, and amphibole contents, in addition to quartz. These phases cover a spectrum of reactivity, from quartz, which is considered close to inert in soil acidity neutralization and does not release ions to increase the pH [63], to albite, a sodium-rich plagioclase feldspar, and epidote, a complex mineral not typically used as a pH corrector that offers moderate neutralizing properties [64]. Although basalt contains minerals that contribute to soil acidity neutralization, the slower dissolution rate of basalt mineral phases compared to olivine and wollastonite and to carbonate-rich minerals implies a gradual release of essential ions for pH neutralization, impacting its short-term and long-term overall effectiveness [65]. The effect is certainly not expected to be nil, and thus basalt as a liming agent can have effectiveness with higher amendment rates or more frequent re-application.

Bentonite is a common term for clayey aluminosilicates from basic minerals [66]. Due to its porosity, high surface area, and silicate layer structure, bentonite acts as a liming material by adsorption/desorption mechanisms rather than reactive weathering. Its composition mainly consists of clays and thus does not contain a significant amount of highly reactive carbonates or silicates that can contribute to soil acidity correction. Therefore, the bentonite sample presented by far the lowest NV (2.51%) among the materials studied.

The low NV value of bentonite helps to reconfirm that the silicate-rich minerals olivine, kimberlite, wollastonite, and basalt have liming potential according to their NV values, even if more attenuated compared to natural limestones. Still, the inconsistency found with wollastonite having an NV value lower than its weathering reactivity would suggest, which may also affect basalt, suggest that the NV test may not be appropriate for all silicates. Hence, there is an opportunity to develop an empirical model that more accurately represents the behavior of silicates in the liming effect.

### 3.1.1. Mineralogical and Morphological Assessments of Digestion Reactions

Figure 2 presents a series of XRD patterns comparing untreated and digested mineral samples. The direct comparison of the before and after diffraction patterns demonstrates which mineral samples reacted extensively, moderately, or minimally. The mineral with the least changes in mineral composition was basalt. In the basalt sample (Figure 2a), peaks corresponding to plagioclase albite (d-spacings ( $I/I_0$ ): 3.176 Å (1), 3.211 Å (0.3), 3.752 Å (0.3)), and quartz (3.342 Å (1), 4.257 Å (0.22), 1.818 Å (0.14)) maintained similar diffraction intensity in the digested sample, while the chlorite chamosite (3.52 Å (1), 7.05 Å (1), 2.52 Å (0.9)) and the amphibole actinolite (8.38 Å (1), 3.12 Å (1), 2.71 Å (0.9)) remained in the digested sample but with attenuated intensity. Conversely, the most significant changes in diffraction patterns were observed with kimberlite. In kimberlite (Figure 2d), the carbonate phases of calcite (3.035 Å (1), 2.095 Å (0.9), 1.871 Å (0.8)) and ankerite (2.899 Å (1), 1.812 Å (0.06), 2.199 Å (0.06)) were fully reacted after digestion, and the digested residue became enriched in serpentine lizardite (7.12 Å (1), 2.379 Å (0.9), 3.56 Å (0.8)) and pyroxene forsterite (4.76 Å (1), 2.70 Å (0.9), 2.52 Å (0.8)). Due to this enrichment, it is not possible to ascertain from XRD alone if these silicate phases in kimberlite reacted. This becomes more evident in the olivine sample. In the case of olivine (Figure 2b), it too reacted extensively, with some phases vanishing or significantly reducing in intensity, including serpentine and chlorite minerals tremolite (8.38 Å (1), 3.12 Å (1), 2.71 Å (0.9)), lizardite and chlinochlore (7.16 Å (1), 4.77 Å (0.7), 3.58 Å (0.6)), and pyroxene forsterite. However, new phases were detected in digested olivine, namely the pyroxenes enstatite (3.167 Å (1), 2.872 Å (0.85), 2.494 Å (0.5)) and hypersthene (3.20 Å (1), 2.70 Å (0.9), 2.50 Å (0.8)). It can thus be inferred that forsterite partly weathered and partly formed secondary minerals through incongruent dissolution; this can happen because ferroan forsterite ( $(\text{Mg,Fe}^{\text{II}})_2\text{SiO}_4$ ) has a 2:1 (Mg,Fe<sup>II</sup>)-to-Si ratio, and hence it can react into simpler silicates with 1:1 ratio of Mg:Si or (Mg,Fe<sup>II</sup>):Si such as enstatite ( $\text{MgSiO}_3$ ) and hypersthene ( $(\text{Mg,Fe}^{\text{II}})\text{SiO}_3$ ). A similar observation is made in the case of wollastonite, but with different mineral phase involvement. In the case of wollastonite (Figure 2c), enstatite formation was also observed in the digested sample, and its origin in the case must be diopside (2.991 Å (1), 2.528 Å (0.4),

2.893 Å (0.3)). But in this case, diopside (MgCaSiO<sub>6</sub>) weathers by releasing its Ca content while the Mg content is inferred to remain in the form of enstatite. Equations (10) and (11) exemplify secondary mineral formation reactions. Enstatite is thermodynamically more stable, so it can eventually weather in a liming application, but in the accelerated digestion reaction, it appears to resist the rapid reaction.

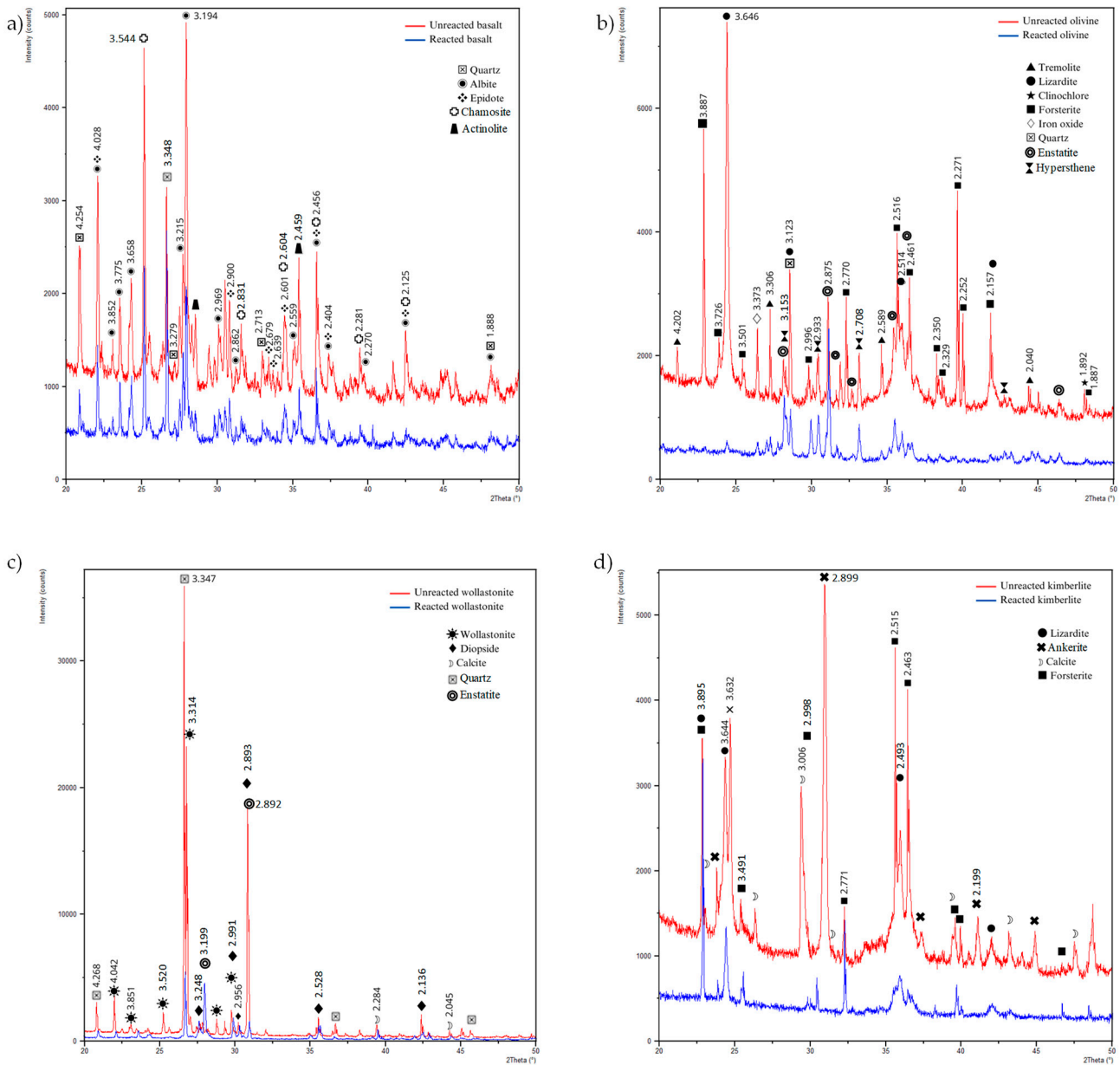
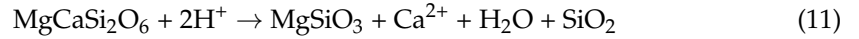
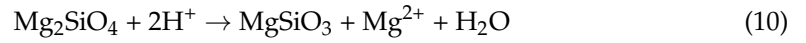


**Figure 2.** XRD patterns of mineral samples comparing untreated (red) and digested (blue), highlighting original mineral phases and changes in (a) basalt, (b) olivine, (c) wollastonite, and (d) kimberlite.

Wollastonite mineral phase (d-spacings ( $I/I_0$ ): 3.314 Å (1), 3.83 Å (0.85), 3.52 Å (0.8)) is unique in having acicular particles, which contributes to this phase being most susceptible to preferential orientation, which causes certain peak intensities to become magnified. In the digested sample, wollastonite peaks are still visible, but peak intensities are much lower. This can signify a combination of mineral dissolution and also attenuation of the

acicularity of the particles (i.e., loss of needle morphology). It is thus critical to also assess particle morphology to better understand reaction effects and extent, which is illustrated for wollastonite in Figure 3. A reduction in the number of visible needles, an alteration in the surface texture of the remaining needles, and a shortening of the remaining needles is seen, supporting the XRD results.

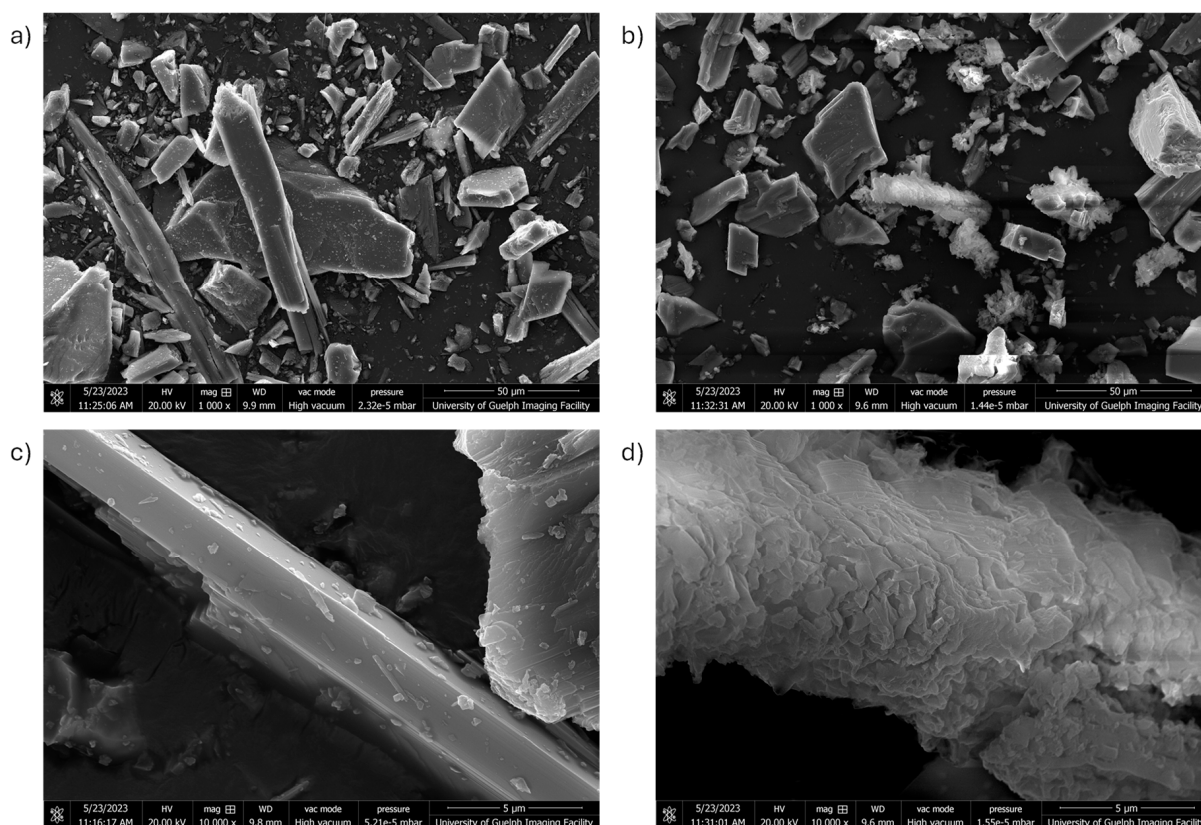


**Figure 3.** Scanning electron microscope (SEM) images showing the surface morphology and particle structures of wollastonite mineral samples at 1000 $\times$  and 10,000 $\times$  magnification, following and prior to digestion. Panels (a,c) depict wollastonite before digestion, and panels (b,d) show wollastonite after digestion.

In Figure 4, the top row (basalt) displays highly fractured and irregularly shaped surfaces, characteristic of comminuted rocks with high porosity and mineral heterogeneity. The digested basalt sample did not display significant morphological changes, apart from possibly the loss of very fine materials that could have reacted away or been lost during filtration. The olivine sample (second row of Figure 4) shows clearer morphological changes, with the surface of most particles (Figure 5) acquiring a rugged texture characteristic of the formation of silica nodules and potentially enstatite byproduct. These surface alterations are similar to those seen in the third row of Figure 4 for wollastonite, and hence are most suggestive of silica (SiO<sub>2</sub>) residue. Enstatite thus is more likely to be found in the interior of particles covered by silica, or as separate particles that do not have a silica layer (as seen in Figure 5). The bottom row in Figure 4 shows kimberlite composed of various types of particles, many of which have porous or fibrous textures. It is unclear from the original sample which particles are the carbonate phases, but what is seen is that in the digested sample the particles suffered from the charging effect, which occurs when the sample is poorly conductive to the electrons of the SEM, despite having been sputter-coated with a conductive layer. Hence this charging behavior is suggestive of mineral reactivity leaving behind loosely bound materials on particles or highly porous structures.

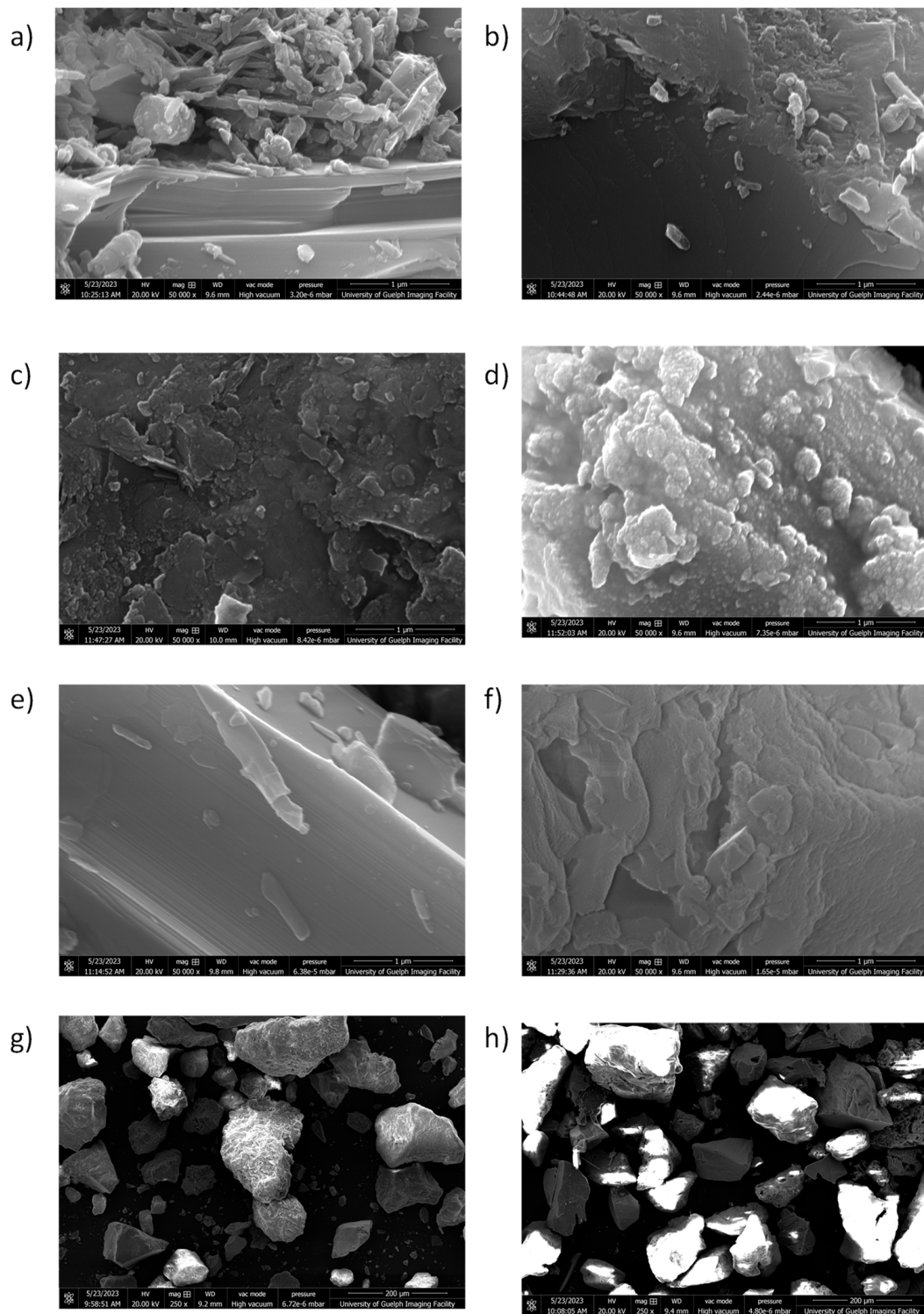


**Figure 4.** Scanning electron microscope (SEM) images showing the surface morphology and particle structures of mineral samples at 50,000 $\times$  and 250 $\times$  magnification, following and prior to digestion. Panels (a,b) depict basalt before and after digestion, respectively. Panels (c,d) show olivine before and after digestion, while (e,f) illustrate wollastonite before and after digestion. Panels (g,h) present kimberlite at a lower magnification of 250 $\times$ , highlighting the surface charging observed during analysis and the varied morphology of its particles.

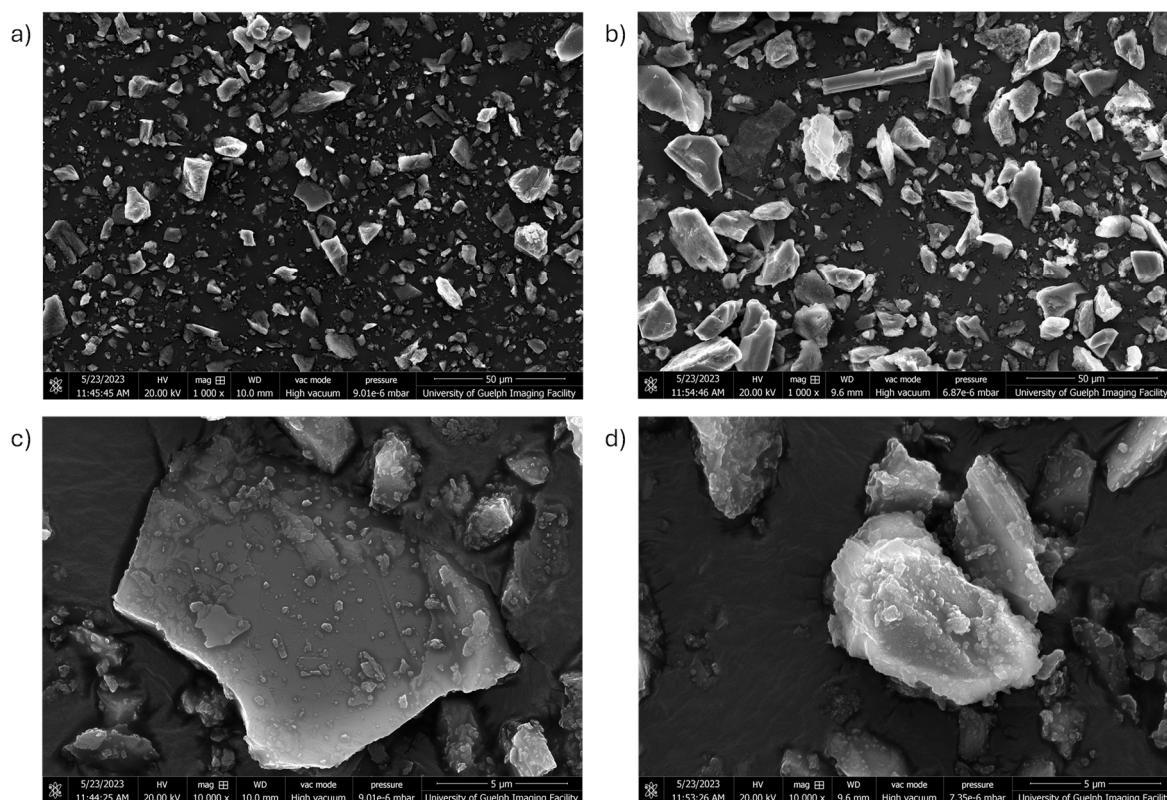


**Figure 5.** Scanning electron microscope (SEM) images showing the surface morphology and particle structures of olivine mineral samples at 1000 $\times$  and 10,000 $\times$  magnification, following and prior to digestion. Panels (a,c) depict olivine before digestion, and panels (b,d) show olivine after digestion.

### 3.2. Pot Test Results

After obtaining incompatible LI values for the studied minerals with their expected reactivity and liming efficiency, we decided to conduct a controlled laboratory experiment. This experiment involved collecting pH data based on variations in dosage and the method of mineral application to the soil in pots. The ultimate objective is to develop an empirical model that more accurately explains the behavior of the minerals under study than the actual LI. As expected, the collected pH data exhibited significant heterogeneity (Figure 6).

In both application methods, calcium carbonate and wollastonite consistently lead to higher pH levels, particularly after SMA, indicating their strong neutralizing capacity. Olivine shows moderate increases, while bentonite consistently results in lower pH levels across all treatments. The comparative trends between mixed and surface applications demonstrate the varying effectiveness of minerals in adjusting soil pH depending on the method and rate of application.

The data collected from the experiment were subjected to nonparametric statistical tests (Wilcoxon, SMA, and Kendall) and significance tests to reliably extract and express the underlying signal.

#### 3.2.1. Wilcoxon

A test was conducted to investigate whether there was a statistically significant difference in pH between the pots, indicating the presence or absence of a liming effect. Compared with those in the soil without minerals, the pH in the soil without minerals significantly differed, confirming a positive liming effect in the pots with added minerals. In contrast, the pH did not significantly differ between soil with added  $\text{CaCO}_3$  and soil with added minerals, indicating similar pH changes and a consistent liming effect among the minerals studied.



**Figure 6.** The plots illustrate the pH changes over time for key minerals (calcium carbonate, bentonite, olivine, and kimberlite) applied through mixed (a,b,e,f) and surface application methods (c,d,g,h), both before (a,c,e,g) and after (b,d,f,h) the implementation of the SMA.

### 3.2.2. SMA, KC, and pH Change Rate

After the Wilcoxon test, we applied a simple moving average (SMA) to smooth the data and better visualize the trend between pot experiments (Figure 6b,d,f,h). The Kendall test was employed for the SMA results to evaluate the hypothesis of correlation and a progressive upward trend in pH during the experiment. Kendall's Tau ( $\tau$ ) value quantifies the strength and direction of the association (agreement or disagreement) between two categorized variables, pH and time of the experiment. Additionally, the pH change rate was calculated for all minerals in both experiments. Table 2 details the  $p$  values, tau values, and pH changes for all the samples.

**Table 2.**  $p$ -values and Tau ( $\tau$ ) values. This table summarizes the  $p$ -values and Tau ( $\tau$ ) values for changes in soil pH following the application of different minerals at various rates and methods (mixed and surface applications). The  $p$ -values indicate the statistical significance of the pH change, while Tau ( $\tau$ ) reflects the magnitude and direction of the change. Data are presented for multiple application rates, with the percentage change in pH noted for each condition.

Mineral	Experiment	Mixed Application				Surface Application			
		Rate 1 $p$ -Value Tau( $\tau$ ) pH Change	Rate 2 $p$ -Value Tau( $\tau$ ) pH Change	Rate 3 $p$ -Value Tau( $\tau$ ) pH Change	Rate 4 $p$ -Value Tau( $\tau$ ) pH Change	Rate 1 $p$ -Value Tau( $\tau$ ) pH Change	Rate 2 $p$ -Value Tau( $\tau$ ) pH Change	Rate 3 $p$ -Value Tau( $\tau$ ) pH Change	Rate 4 $p$ -Value Tau( $\tau$ ) pH Change
Bentonite	1	0.015	0.0221	0.116	0.435	0.100	0.100	0.076	0.057
		0.513 13%	0.487 11%	0.582 8%	0.179 5%	0.359 8%	0.3759 7%	0.385 11%	0.410 4%
	2	0.000	0.000	0.000	0.036	0.001	0.000	0.000	0.001
		0.760 3%	0.636 1%	0.669 2%	0.347 1%	0.536 3%	0.820 3%	0.675 2%	0.507 0%
Basalt	1	0.435	0.252	0.030	0.000	0.076	0.004	0.000	0.001
		-0.179 3%	0.256 9%	0.462 9%	0.846 9%	0.385 12%	0.590 15%	0.876 10%	0.692 12%
	2	0.000	0.000	0.000	0.000	0.000	0.000	0.322	0.078
		0.773 2%	0.782 3%	0.732 3%	0.544 1%	0.547 2%	0.812 2%	0.159 0%	0.278 0%
Wollastonite	1	0.099	0.003	0.760	0.675	0.007	0.765	0.127	0.252
		0.348 13%	0.632 16%	0.065 11%	0.103 10%	0.564 14%	-0.077 7%	0.323 8%	0.256 5%
	2	0.000	0.000	0.001	0.000	0.081	0.016	0.000	0.000
		0.780 2%	0.789 3%	0.538 1%	0.633 1%	0.293 1%	0.385 1%	0.601 2%	0.738 2%
Kimberlite	1	0.367	0.367	0.306	0.435	0.030	0.004	0.002	0.590
		0.205 8%	-0.205 3%	0.231 6%	-0.179 7%	0.462 11%	0.590 10%	0.658 13%	0.128 10%
	2	0.000	0.000	0.000	0.000	0.000	0.020	0.000	0.000
		0.771 2%	0.794 3%	0.868 3%	0.591 0%	0.843 4%	0.374 1%	0.527 0%	0.796 10%
Olivine	1	0.003	0.030	0.197	0.164	0.002	0.858	0.001	0.010
		0.615 8%	0.462 11%	0.275 8%	0.308 8%	0.641 10%	-0.051 13%	0.667 12%	0.538 12%
	2	0.000	0.000	0.001	0.004	0.000	0.010	0.051	0.099
		0.796 3%	0.826 1%	0.548 0%	-0.458 -1%	0.806 2%	0.419 1%	0.312 1%	0.269 -1%
Calcium carbonate	1	0.160	0.076	0.044	0.367	0.000	0.001	0.000	0.952
		0.297 6%	0.374 9%	0.426 12%	0.205 10%	0.744 12%	0.675 11%	0.872 13%	0.026 9%
	2	0.001	0.931	0.548	0.380	0.134	0.531	0.173	0.350
		0.556 0%	-0.014 -1%	0.095 0%	0.137 0%	0.242 3%	0.099 2%	0.219 4%	0.145 3%

### 3.2.3. Data Filtering

To determine the most significant set of pH values for calculating the pH slope, we employed the following selection criteria: only pH values with a statistically significant difference ( $p$ -value less than 0.05) were considered; preference was given to pH values demonstrating a high Kendall's Tau ( $\tau$ ), indicating a strong monotonic relationship; and values with the lowest rate of change in pH were prioritized. The pH values meeting these criteria are highlighted in bold in Table 2.



### 3.3. Ranking Performed Using Neutralizing Values

The slopes of the filtered minerals ( $Rank(S_{pH_i})$ ) were calculated and organized in descending order of values (ranking) considering the method of application (surface and mixed) and all pots. Additionally, the same is true for the NV values  $Rank(NV_i)$  see Table 3. Afterwards, the difference between them was calculated ( $Rank(S_{pH_i}) - Rank(NV_i)$ ); see Table 4. Since this term in the equation is different from zero, it indicates a discrepancy between the experimental value and that predicted by NV, confirming our hypothesis that NV is not a reliable predictor. This leads us to the next stage of the work, where we develop a preliminary empirical model that presents a reduced difference.

Table 3 presents a comprehensive comparison of various minerals based on their empirical model data, neutralizing value (NV), and experimental results, specifically focusing on the slope of the pH change. The table provides a detailed analysis of each mineral's performance in surface and mixed applications, ranking them accordingly. The ranking system facilitates the comparison between the liming effectiveness noted by NV, the empirical model data, and the experimental results.

Table 4 provides a detailed ranking analysis for various minerals based on their performance in different experimental setups. The table uses a weighted ranking system to compare the experimental results against the empirical model data and neutralizing value (NV).

### 3.4. Empirical Modeling

Table 5 provides detailed empirical data for the various samples used in this study. The table includes parameters related to dosage, reactivity rate, BSSA, GSSA, purity, and molar mass. The  $Wr$  is reported in square meters per mole per second and is based on the neutral mechanism (25 °C, pH = 7) [43]. The specific surface area (SSA) is reported in square meters per gram. We adjusted the SSA for the molar mass in each mineral, measured in square meters per mole. The final value [ $\log(SSA \times Wr)$ ] represents the logarithm of the product of the specific surface area and weathering rate  $Wr$ .

Figure 7 illustrates the relationship between the mineral dosage and the empirical model results for various minerals and two types of specific surface area (SSA) measurements. The x-axis represents the mineral dosage in grams, ranging from 0 to 16 g, while the y-axis represents the logarithm of ( $SSA \times Wr$ ), ranging from  $-7$  to  $-17$ . The plot includes two sets of data points and their corresponding logarithmic trend lines with equations and  $R^2$  values. The trend lines show a general decreasing trend in [ $\log(SSA \times Wr)$ ] values as the mineral dosage increases. This is consistent with the current understanding that minerals with lower reactivity require a higher dosage to achieve a similar liming effect. The dataset based on the BSSA ( $\log(BSSA \times Wr)$ ) has a slightly better fit ( $R^2 = 0.8139$ ) with the logarithmic model than does the GSSA dataset ( $R^2 = 0.5735$ ). However, the GSSA equation has a greater coefficient for  $x^2$  and  $x$  and a greater negative coefficient for  $x$ , which means that the curvature and slope are steeper than those of the BSSA equation. This indicates that the empirical model using GSSA is more sensitive to dosage variations. For this reason, we decided to adopt the GSSA as our reference for the preliminary empirical model. Additionally, the higher reactivity of calcium carbonate at a lower dosage highlights its potential efficiency in such processes, whereas the lower reactivity of bentonite at a higher dosage suggests that it may be less effective under sim. Overall, this empirical model helps in understanding the reactivity of different minerals at varying dosages, which is crucial for applications in fields such as soil amendment, carbon sequestration, and enhanced weathering.

**Table 3.** Mineral reactivity and impact on soil pH for different application methods. This table displays the neutralizing value (NV) of various minerals, expressed as % equivalent CaCO<sub>3</sub>, alongside their reactivity measured by log(GSSA × Wr). It includes rankings for each mineral based on NV(Rank(NV<sub>i</sub>)), empirical method EM (Rank(EM<sub>i</sub>)), and pH slope changes in soil (Rank(S<sub>pHi</sub>)), highlighting their performance and impact on pH adjustment.

Mineral	NV (%Eq CaCO <sub>3</sub> )	EM <sub>i</sub> (Log [GSSA × Wr])	Experiment	Surface Application	Mixed Application	All Pots	Surface Application	Mixed Application	All Pots	
				Slope pH	Slope pH	Slope pH	Rank (NV <sub>i</sub> )	Rank (EM <sub>i</sub> )	Rank (S <sub>pHi</sub> )	Rank (S <sub>pHi</sub> )
Bentonite	2.509	−13.386	1	0.0821	0.0753	0.0787				
			2	0.0120	0.0343	0.0232	6	6	6	
Wollastonite	20.818	−12.486	1	0.1084	0.0597	0.0841	5	2	3	
			2	0.1029	0.0713	0.0871		3	4	4
Basalt	25.630	−13.142	1	0.0852	0.1030	0.0941		4	2	2
			2	0.0464	0.0443	0.0464	4	5	5	5
Kimberlite	61.993	−12.501	1	0.1043	0.1043	0.1043		3	1	1
			2	0.0907	0.1052	0.0979	3	3	4	3
Olivine	74.254	−12.895	1	0.0651	0.0570	0.0610		6	5	6
			2	0.1437	0.1072	0.1072	2	4	2	2
CaCO <sub>3</sub>	103.160	−8.532	1	0.1129	0.0533	0.0831	1	1	6	4
			2	0.2002	0.1198	0.1600		1	1	1

**Table 4.** Comparative ranking and weighted scores for soil pH adjustment of different minerals by application method. This table shows the ranking and weighted scores of various minerals based on their impact on soil pH, assessed through surface and mixed applications. It includes weighted differences between ranks for pH slope changes, mineral effectiveness, and neutralizing value (NV), providing a comprehensive evaluation of each mineral’s performance across different experimental conditions. For this time, it was set α = γ = 1.

Mineral	Experiment	Surface Application			Mixed Application			Total		
		$(\alpha *  Rank(S_{pHi}) - Rank(NV_i) ) / Rank(ME_i)$	$(\gamma *  Rank(S_{pHi}) - Rank(NV_i) )$	Rank <sub>i</sub>	$(\alpha *  Rank(S_{pHi}) - Rank(NV_i) ) / Rank(ME_i)$	$(\gamma *  Rank(S_{pHi}) - Rank(NV_i) )$	Rank <sub>i</sub>	$(\alpha *  Rank(S_{pHi}) - Rank(NV_i) ) / Rank(ME_i)$	$(\gamma *  Rank(S_{pHi}) - Rank(NV_i) )$	Rank <sub>i</sub>
Bentonite	1	1	1	3	3	1	1	1	1	
	2	0	0	0	0	0	0	0	0	
Wollastonite	1	0	3	2	1	1	2	2	2	
	2	1	2	2	1	1	1	1	1	
Basalt	1	1	0	3	2	3	2	2	2	
	2	0	1	0	1	0	1	0	1	
Kimberlite	1	0	0	2	2	2	2	2	2	
	2	1	1	0	0	1	0	1	0	
Olivine	1	2	4	1	3	2	4	4	4	
	2	2	0	2	0	0	0	0	0	
Calcite	1	0	0	5	5	3	3	3	3	
	2	0	0	0	0	0	0	0	0	
Sum (Σ)	1	4	8	4	16	16	14	14	12	
	2	4	4	4	4	2	2	2	2	

**Table 5.** Reactivity and physical properties of soil treatment minerals. This table details the properties and reactivity of various minerals used in soil treatments, including dosage, specific surface area (GSSA and BSSA), purity, molar mass, and calculated reaction rates. The log-transformed reaction rates ( $\log(\text{GSSA} \times \text{Wr})$  and  $\log(\text{BSSA} \times \text{Wr})$ ) are also presented to highlight differences in mineral reactivity.

Sample	More Reactive Mineral	Dosage	Log Wr	G SSA	B SSA	Purity	Molar Mass	Molar Mass × Purity	G SSA	B SSA	log (G SSA × Wr)	log (B SSA × Wr)
		g/pot	(mol/(m <sup>2</sup> ·s))	(m <sup>2</sup> /g)	(m <sup>2</sup> /g)	%	(g/mol)	(g/mol)	(m <sup>2</sup> /mol)	(m <sup>2</sup> /mol)	1/s	1/s
Calcium carbonate	Calcium carbonate	3.911	−5.810	0.1518	0.805	80	100.070	80.056	0.0019	0.010	−8.532	−7.808
Kimberlite	Ankerite	6.520	−8.600	0.0107	15.578	30	284.696	85.409	0.00013	0.182	−12.501	−9.339
Olivine	Forsterite	9.056	−10.071	0.1939	4.568	80	161.879	129.503	0.0015	0.035	−12.895	−11.523
Wollastonite	Wollastonite	11.304	−8.320	0.0066	0.198	55	183.550	97.373	0.00007	0.002	−12.486	−11.012
Basalt	Anorthite	13.118	−9.110	0.0157	0.746	40	438.100	168.669	0.00009	0.004	−13.142	−11.464
Bentonite	Montmorillonite	13.402	−12.780	0.1500	62.0	50	242.337	121.169	0.00124	0.512	−13.386	−13.071

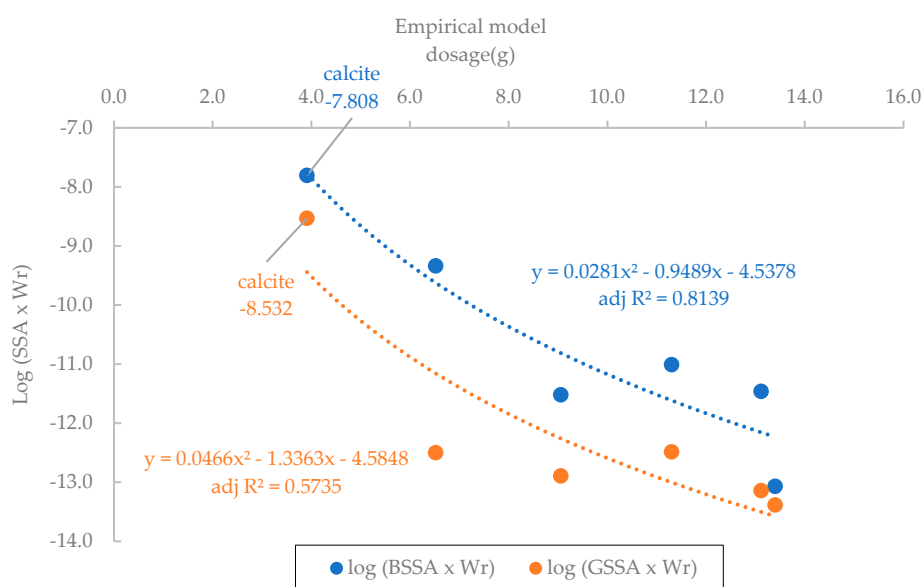


**Figure 7.** Empirical models versus dosage. This plot compares the empirical models for bet surface area (BSSA) and geometric surface area (GSSA) with varying dosages, assessing their reactivity in terms of the product of SSA (BSSA or GSSA) and weathering rate (Wr). The models reveal that the BSSA-based approach (blue) predicts reactivity more accurately ( $\text{adj } R^2 = 0.8139$ ) than the GSSA-based method (orange), which has a lower adjusted  $R^2$  of 0.5735. Both models show decreasing reactivity with increasing dosage, although the rate of decline differs.

### 3.5. Ranking Using an Empirical Model

The empirical values ( $\log(\text{GSSA} \times \text{Wr})$ ) were calculated for each mineral studied. We arranged them in descending order of values ( $\text{Rank}(EM_i)$ ) (see Table 4) and calculated the difference between the slope and the empirical model ( $|\text{Rank}(S_{pH_i}) - \text{Rank}(EM_i)|$ ). The empirical method yielded slightly better results than did the neutralizing value for the selected minerals. Looking at the sum of the rank differences ( $\Sigma$ ) for experiments 1 and 2, we can observe the following: for surface application, the empirical model outperforms the NV method in Experiment 1 and performs equally well in Experiment 2. Regarding mixed application, the empirical model ties with NV in Experiment 1 but falls short in Experiment 2. Overall, without considering the type of application, the empirical model demonstrated superior predictive capability compared to NV in Experiment 1 and matched NV's performance in Experiment 2.

#### 4. Discussion

This study reaffirmed calcium carbonate's status as the benchmark liming material, consistently demonstrating the highest neutralizing value (NV) at 103.16%. This high NV underscores its effectiveness in neutralizing soil acidity, making it a widely used agent in agriculture. Calcium carbonate has been extensively studied for its long-term effects on soil fertility and crop yields. Research indicates that calcium-based liming materials not only neutralize soil acidity but also improve soil structure and enhance the bioavailability of essential nutrients such as calcium, magnesium, phosphorus, and molybdenum [67]. However, the use of calcium carbonate is at times reported to lead to increased leaching of organic matter, which may affect soil organic carbon levels over time, as discussed by Olego et al. [68]. This dual effect underscores the need for balanced application rates and monitoring to optimize soil health and crop productivity.

The exploration of alternative silicate minerals revealed varied neutralizing potentials, highlighting the complexity of their interactions with soil. Olivine, despite its slower dissolution rates compared to carbonates, exhibited significant NV values (59.33% eq  $\text{CaCO}_3$  by Method A and 74.25% eq  $\text{CaCO}_3$  by Method B). This is likely due to the release of magnesium ions during weathering, which contributes to its neutralizing capacity. However, the presence of nickel ions in olivine may limit its agricultural use due to potential toxicity, necessitating careful consideration of its application. Rietra [69] reported poor liming performance of olivine versus dolomitic limestone, suggesting that the former has a liming efficiency that is 35 smaller than the latter, despite having an NV of 36.4% eq  $\text{CaCO}_3$  versus 50% of the reference carbonate. The study attributed the difference in performance to the slower reactivity of olivine as inferred by potentiometric titration. Still, the soil tests conducted showed a pH change of 0.2 to 0.6 units for the use of 2 to 6 wt% olivine in soil, highlighting that the target pH change, and the duration of the pH effect, as additional parameters to consider when comparing long-term liming efficiency and carbon footprint.

Kimberlite samples showed varying NV results, with notable discrepancies between methods indicating iron interference in the NV analysis. The presence of calcite and other magnesium silicate minerals contributed to its NV. While kimberlite has the potential to improve soil quality and provide essential nutrients, careful management and monitoring are necessary to mitigate the risks associated with heavy metal contamination, such as nickel and chromium. Conducting thorough research and pilot projects can help determine its feasibility as a soil amendment in Ontario.

Basalt, a volcanic rock rich in silicate minerals, is widely considered for enhanced rock weathering (ERW) due to its abundance and effectiveness in reacting with  $\text{CO}_2$ . Studies have shown that basalt can significantly contribute to carbon sequestration by converting atmospheric  $\text{CO}_2$  into stable bicarbonates, which are eventually transported to the oceans [70]. This process not only aids in carbon removal but also improves soil health by supplying essential minerals and correcting soil pH levels [71]. However, our results indicate that basalt has a limited liming efficiency with an NV of 13.14% eq  $\text{CaCO}_3$ . This is attributed to its mineral composition, including albite, quartz, and epidote, which contribute to its slow dissolution rate and minimal effective carbonate minerals. Despite its potential for carbon sequestration, basalt's effectiveness as a liming agent is limited, suggesting that its primary benefit in agriculture may lie more in its role in ERW rather than soil pH correction [72]. Similarly, bentonite, a clay-rich mineral, had the lowest NV (2.51% eq  $\text{CaCO}_3$ ), relying on adsorption rather than weathering, with a composition lacking significant calcium or magnesium carbonate content.

Unexpectedly, wollastonite samples had lower-than-expected NV (19.85% eq  $\text{CaCO}_3$ ). This can be explained by the phenomenon of passivation during the carbonation process. Passivation occurs when a protective layer, often composed of amorphous silica, forms on the surface of the dissolving mineral, inhibiting further dissolution and reaction. Despite its theoretically high reactivity due to fast-weathering calcium silicate, the actual NV observed

is lower because of the passivation effect. This finding highlights the importance of considering passivation effects in predicting the carbonation potential and NV of minerals.

The empirical model developed in this study offers a more comprehensive approach to predicting liming efficiency compared to the traditional liming index (LI) test. While the LI test primarily measures the potential of a mineral to neutralize acidity based on its calcium carbonate equivalent, it does not account for factors such as surface area, weathering rate, and mineralogical properties. Our empirical model integrates these parameters, providing a more nuanced understanding of mineral behavior under specific conditions [73]. By including the product of specific surface area (SSA) and weathering rate ( $Wr$ ), the model captures the reactivity of a mineral more accurately. Additionally, the model's ability to adjust for mineral dosage and integrate multiple variables leads to a more robust and versatile prediction of liming efficiency. This approach aligns more closely with experimental results, particularly in terms of pH change slopes observed in surface and mixed applications, demonstrating its effectiveness in real-world scenarios [74].

The empirical model's better fit can be attributed to several key factors:

1. **Surface Area and Weathering Rate:** The empirical model includes the product of the specific surface area (SSA) and weathering rate ( $Wr$ ), which is crucial because the reactivity of a mineral depends significantly on its surface area available for reaction. By adjusting SSA for molar mass and calculating the logarithm of the product ( $\log(SSA \times Wr)$ ), the model captures how these factors influence reactivity, which NV alone does not address.
2. **Mineral Dosage Sensitivity:** The empirical model shows that reactivity changes with mineral dosage. It highlights that as dosage increases, the reactivity decreases, especially for less reactive minerals, which aligns with the trend observed in the data.
3. **Multi-Parameter Integration:** The empirical model synthesizes multiple variables, including reactivity rate, surface area, and mineralogical properties, leading to a more robust and versatile prediction. In contrast, NV focuses solely on the acid-neutralizing capacity, overlooking the complexities of mineral reactivity under different conditions.
4. **Experimental Validation:** The empirical model's predictive capability aligns more closely with experimental results, particularly in terms of pH change slopes observed in surface and mixed applications. The model's ability to reflect actual performance better than NV demonstrates its effectiveness in real-world scenarios.

## 5. Conclusions

The pH of the soil is critical for plant growth and nutrient availability. Soil acidity can lead to land degradation and impact agricultural productivity. Several factors, such as acidic precipitation and the use of ammonium-based fertilizers, contribute to soil acidity. Soil amendments, particularly liming agents such as limestone ( $CaCO_3$ ), are used to neutralize soil acidity and enhance nutrient availability [5]. Despite their effectiveness, the use of liming agents can lead to  $CO_2$  emissions due to reactions with strong acids in the soil. In this work, silicate minerals were investigated as alternative liming agents. The use of silicate minerals can contribute to long-term soil health by enhancing soil structure and fertility while reducing  $CO_2$  emissions associated with traditional liming agents [75]. This study investigated silicate minerals as alternative liming agents, which can enhance soil structure and fertility while reducing  $CO_2$  emissions.

The empirical model developed in this study showed superior predictive capability compared to the NV method, particularly in surface applications. It integrates parameters such as weathering rate, specific surface area, and molar mass, providing a more nuanced understanding of mineral behavior. This model better fits experimental results, reflecting actual performance more accurately than the NV method.

In summary, the empirical model offers a more detailed and accurate prediction of mineral behavior by incorporating critical factors like surface area, reactivity rates, and dosage effects. This study provides valuable data for developing guidelines on the

appropriate use of silicate minerals in agriculture. Farmers can use the empirical model to optimize soil pH and nutrient availability.

Further research is needed to refine the empirical model and explore the long-term effects of silicate mineral amendments on soil health and crop productivity. Future studies should also investigate the environmental impact of large-scale silicate mineral application in different agricultural settings.

This study highlights important agronomic benefits, emphasizing that farmers should optimize lime application rates based on soil types and pH needs to avoid both over-application, which wastes resources, and under-application, which may not sufficiently address soil acidity. Adopting site-specific management practices, considering factors like soil texture, organic matter, and historical cultivation, maximizes the benefits of liming while reducing costs. Regular soil testing is essential for monitoring pH and nutrient availability, ensuring lime is applied when necessary and in appropriate amounts. Integrating lime into crop rotation cycles can help maintain optimal soil pH and support long-term productivity. Farmers should also be mindful of the environmental impact, avoiding over-liming, which can disrupt soil balance and sustainability.

Additionally, this study encourages authorities to play a pivotal role in promoting sustainable liming practices. Governments should support soil testing programs, enabling farmers to make informed decisions about lime application. Agricultural extension services should offer training on proper lime usage and how to interpret soil test results. Authorities are also encouraged to regulate lime quality, promote sustainable agricultural practices, and invest in research to develop more efficient liming materials and techniques. This approach will help improve agricultural yields while minimizing environmental impacts.

In conclusion, this study highlights the potential of silicate minerals as effective liming agents, offering a sustainable alternative to traditional carbonates. By incorporating these findings into agricultural practices, farmers can achieve better soil management, enhance crop yields, and contribute to environmental sustainability.

**Author Contributions:** Conceptualization, F.S.M.A. and R.M.S.; methodology, F.S.M.A., A.G.M.C., R.F.P. and R.M.S.; software, F.S.M.A., J.P.L.C.; investigation, F.S.M.A., A.G.M.C. and R.F.P.; resources, Y.W.C. and R.M.S.; data curation, F.S.M.A.; writing—original draft preparation, F.S.M.A.; writing—review and editing, R.M.S.; supervision, Y.W.C. and R.M.S.; project administration, Y.W.C. and R.M.S.; funding acquisition, Y.W.C. and R.M.S. All authors have read and agreed to the published version of the manuscript.

**Funding:** This research was partly supported by the Mitacs Globalink program, and by the Emerging Leaders in the Americas Program (ELAP).

**Data Availability Statement:** The raw data supporting the conclusions of this article will be made available by the authors on request.

**Acknowledgments:** The authors thank the assistance provided by the University of Guelph Phytotron facility.

**Conflicts of Interest:** The authors declare no conflicts of interest.

## References

1. Buni, A. Effects of liming acidic soils on improving soil properties and yield of haricot bean. *J. Environ. Anal. Toxicol.* **2014**, *5*, 1–4. [[CrossRef](#)]
2. Goulding, K. Soil acidification and the importance of liming agricultural soils with particular reference to the United Kingdom. *Soil Use Manag.* **2016**, *32*, 390–399. [[CrossRef](#)] [[PubMed](#)]
3. Van Der Bauwhede, R.; Troonbeeckx, J.; Serbest, I.; Moens, C.; Desie, E.; Katzensteiner, K.; Van-campenhout, K.; Smolders, E.; Muys, B. Restoration rocks: The long-term impact of rock dust application on soil, tree foliar nutrition, tree radial growth, and understory biodiversity in Norway spruce forest stands. *For. Ecol. Manag.* **2024**, *568*, 122109. [[CrossRef](#)]
4. West, T.O.; McBride, A.C. The contribution of agricultural lime to carbon dioxide emissions in the United States: Dissolution, transport, and net emissions. *Agric. Ecosyst. Environ.* **2005**, *108*, 145–154. [[CrossRef](#)]
5. Li, Y.; Cui, S.; Chang, S.X.; Zhang, Q. Liming effects on soil pH and crop yield depend on lime material type, application method and rate, and crop species: A global meta-analysis. *J. Soils Sediments* **2019**, *19*, 1393–1406. [[CrossRef](#)]

6. Ontario Ministry of Agriculture, Food and Rural Affairs. Agronomy Guide for Field Crops (Publication 811). *Ontario Ministry of Agriculture Food and Rural Affairs*. 2022. Available online: <https://www.ontario.ca/files/2022-10/omafra-agronomy-guide-for-field-crops-en-2022-10-13.pdf> (accessed on 6 September 2024).
7. Drapanauskaitė, D. Effect of Different Chemical Composition and Structure of Liming Materials on Acid Soil Neutralizing. Ph.D. Dissertation, Vytautas Magnus University, Lithuanian Research Centre for Agriculture and Forestry, Kauno, Lithuania, 2020. Available online: <https://www.lammc.lt/data/public/uploads/2020/11/donatos-drapanauskaites-disertacija.pdf> (accessed on 6 September 2024).
8. Van Der Bauwhede, R.; Muys, B.; Vancampenhout, K.; Smolders, E. Accelerated weathering of silicate rock dusts predicts the slow-release liming in soils depending on rock mineralogy, soil acidity, and test methodology. *Geoderma* **2024**, *441*, 116734. [[CrossRef](#)]
9. Ramos, C.G.; Hower, J.C.; Blanco, E.; Oliveira, M.L.S.; Theodoro, S.H. Possibilities of using silicate rock powder: An overview. *Geosci. Front.* **2022**, *13*, 101185. [[CrossRef](#)]
10. Alcarde, J.C.; Rodella, A. O equivalente em carbonato de cálcio dos corretivos da acidez dos solos. *Sci. Agric.* **1996**, *53*, 204–210. [[CrossRef](#)]
11. ISO 20978:2020; Liming Material—Determination of Neutralizing Value—Titrimetric Methods. International Organization for Standardization: Geneva, Switzerland, 2020. Available online: <https://www.iso.org/standard/69678.html> (accessed on 6 September 2024).
12. Paradelo Núñez, R.; Virto, I.; Chenu, C. Net effect of liming on soil organic carbon stocks: A review. *Agric. Ecosyst. Environ.* **2015**, *202*, 98–107. [[CrossRef](#)]
13. Caires, E.F.; Garbuio, F.J.; Churka, S.; Barth, G.; Correa, J.C.L. Effects of lime and gypsum on soil acidity and crop yield in a no-till system. *Field Crops Res.* **2005**, *92*, 177–185. [[CrossRef](#)]
14. Tang, C.; Rengel, Z.; Diatloff, E.; Gazey, C. Impact of lime on plant growth and soil organic matter in acidic soils. *Plant Soil* **2003**, *253*, 231–242.
15. Arshad, M.A.; Soon, Y.K.; Azooz, R.H.; Lupwayi, N.Z. Soil and crop response to wood ash and lime application in acidic soils. *Agron. J.* **2012**, *104*, 715–721. [[CrossRef](#)]
16. Sale, P.W.G.; Aye, N.S.; Tang, C. Long-term impact of lime on soil organic carbon and aggregate stability. *Soil Res.* **2015**, *53*, 881–890.
17. Crusciol, C.A.C.; Soratto, R.P.; Castro, G.S.A.; Costa, C.H.M.; Neto, J.F.; Franzluebbbers, A.J. Effects of lime and phosphogypsum on soil properties and wheat response in tropical no-till soil. *Soil Sci. Soc. Am. J.* **2011**, *75*, 1040–1048.
18. Doe, J.; Smith, A.; Johnson, B. Silicate minerals as soil amendments: A review. *Soil Sci. Soc. Am. J.* **2020**, *84*, 123–135.
19. Brown, C.; Wilson, D. Effectiveness of silicate-based liming materials in acid soil amelioration. *Agric. Ecosyst. Environ.* **2019**, *279*, 45–53. [[CrossRef](#)]
20. Martinez, E.; Taylor, F. The role of silicates in soil pH regulation and carbon sequestration. *Geoderma* **2021**, *385*, 114–125.
21. Clark, G.; Lee, H. Utilizing silicates as liming agents to improve soil fertility in acidic soils. *J. Soil Water Conserv.* **2018**, *73*, 291–299.
22. Wilkin, R.T.; DiGiulio, D.C. Geochemical impacts to groundwater from geologic carbon sequestration: Controls on pH and inorganic carbon concentrations from reaction path and kinetic modeling. *Environ. Sci. Technol.* **2010**, *44*, 4821–4827. [[CrossRef](#)]
23. Bandyopadhyay, J.; Al-Thabaiti, S.A.; Ray, S.S.; Basahel, S.N.; Mokhtar, M. Unique cold-crystallization behavior and kinetics of biodegradable poly[(butylene succinate)-co-adipate] nanocomposites: A high-speed differential scanning calorimetry study. *Macromol. Mater. Eng.* **2014**, *299*, 939–952. [[CrossRef](#)]
24. Kittridge, M.G. Investigating the influence of mineralogy and pore shape on the velocity of carbonate rocks: Insights from extant global datasets. *Interpretation* **2015**, *3*, SA15–SA31. [[CrossRef](#)]
25. Filipek, T. Liming: Effects on soil properties. In *Soil and Environmental Quality*; Springer: Berlin/Heidelberg, Germany, 2011; pp. 631–646. [[CrossRef](#)]
26. Hou, J.; Liu, Q. Theoretical models and experimental determination methods for equations of state of silicate melts: A review. *Sci. China Earth Sci.* **2019**, *62*, 751–770. [[CrossRef](#)]
27. te Pas, E.E.E.M.; Hagens, M.; Comans, R.N.J. Assessment of the enhanced weathering potential of different silicate minerals to improve soil quality and sequester CO<sub>2</sub>. *Front. Clim.* **2023**, *4*, 954064. [[CrossRef](#)]
28. Agriculture Victoria. Soil Acidity. Department of Agriculture and Rural Development, Victoria. Available online: <https://agriculture.vic.gov.au/farm-management/soil/soil-acidity> (accessed on 6 September 2024).
29. Grunthal, P.E. Investigation of the Utilization of Crumb Rubber and Other Materials as a Waste-Based Soil Amendment for Sports Turf. Master’s Thesis, University of Guelph, Guelph, ON, Canada, 1996.
30. Swoboda, P.; Döring, T.F.; Hamer, M. Remineralizing soils? The agricultural usage of silicate rock powders: A review. *Sci. Total Environ.* **2022**, *807 Pt 3*, 150976. [[CrossRef](#)]
31. Environment and Climate Change Canada. Historical Data. Government of Canada. Available online: [https://climate.weather.gc.ca/historical\\_data/search\\_historic\\_data\\_e.html](https://climate.weather.gc.ca/historical_data/search_historic_data_e.html) (accessed on 6 September 2024).
32. Zárte-Valdez, J.L.; Zasoski, R.J.; Läuchli, A. Short-term effects of moisture content on soil solution pH and soil Eh. *Soil Sci.* **2006**, *171*, 423–431. [[CrossRef](#)]
33. ASTM D4972-01; Standard Test Method for pH of Soils. ASTM International: West Conshohocken, PA, USA, 2001. [[CrossRef](#)]

34. Alloway, B.J. Sources of heavy metals and metalloids in soils. In *Heavy Metals in Soils: Trace Metals and Metalloids in Soils and Their Bioavailability*; Alloway, B.J., Ed.; Springer: Berlin/Heidelberg, Germany, 2012; pp. 11–50. [CrossRef]
35. Hobara, S.; Kushida, K.; Kim, Y.; Koba, K.; Lee, B.-Y.; Ae, N. Relationships among pH, minerals, and carbon in soils from tundra to boreal forest across Alaska. *Ecosystems* **2016**, *19*, 1111–1127. [CrossRef]
36. Wei, Y.-M.; Chen, K.; Kang, J.-N.; Chen, W.; Wang, X.-Y.; Zhang, X. Policy and management of carbon peaking and carbon neutrality: A literature review. *Engineering* **2022**, *14*, 52–63. [CrossRef]
37. Shukla, M.K.; Lal, R.; Ebinger, M. Determining soil quality indicators by factor analysis. *Soil Tillage Res.* **2006**, *87*, 194–204. [CrossRef]
38. Zeraatpisheh, M.; Ayoubi, S.; Sulieman, M.; Rodrigo-Comino, J. Determining the spatial distribution of soil properties using environmental covariates and multivariate statistical analysis: A case study in semi-arid regions of Iran. *J. Arid Land* **2019**, *11*, 551–566. [CrossRef]
39. Silva-Parra, A.; Colmenares-Parra, C.; Álvarez-Alarcón, J. Análisis multivariado de la fertilidad de los suelos en sistemas de café orgánico en puente abadia, villavicencio. *Rev. U.D.C.A. Actual. Divulg. Científica* **2017**, *20*, 289–298. Available online: <http://ref.scielo.org/9zy73r> (accessed on 6 September 2024).
40. Nassiri, O.; Rhoujjati, A.; EL Hachimi, M.L. Contamination, sources and environmental risk assessment of heavy metals in water, sediment and soil around an abandoned Pb mine site in North East Morocco. *Environ. Earth Sci.* **2021**, *80*, 96. [CrossRef]
41. Zhang, H.; Cause and Effects of Soil Acidity (Oklahoma State University Extension Fact Sheet PSS-2239). Oklahoma State University Extension. 2017. Available online: <https://extension.okstate.edu/fact-sheets/cause-and-effects-of-soil-acidity.html> (accessed on 6 September 2024).
42. Zhao, K.; Fu, W.; Qiu, Q.; Ye, Z.; Li, Y.; Tunney, H.; Dou, C.; Zhou, K.; Qian, X. Spatial patterns of potentially hazardous metals in paddy soils in a typical electrical waste dismantling area and their pollution characteristics. *Geoderma* **2019**, *337*, 453–462. [CrossRef]
43. Palandri, J.L.; Kharaka, Y.K. *A Compilation of Rate Parameters of Water-Mineral Interaction Kinetics for Application to Geochemical Modeling*; U.S. Geological Survey Open-File Report of 2004-1068; National Energy Technology Laboratory—United States Department of Energy: Menlo Park, CA, USA, 2004. Available online: <https://pubs.usgs.gov/of/2004/1068/> (accessed on 6 September 2024).
44. Haque, F.; Khalidy, R.; Chiang, Y.W.; Santos, R.M. Constraining the capacity of global croplands to CO<sub>2</sub> drawdown via mineral weathering. *ACS Earth Space Chem.* **2023**, *7*, 1294–1305. [CrossRef]
45. ISO 13320:2020; Particle Size Analysis—Laser Diffraction Methods. ISO: Geneva, Switzerland, 2020. Available online: <https://www.iso.org/standard/69111.html> (accessed on 6 September 2024).
46. Crundwell, F.K. The mechanism of dissolution of forsterite, olivine and minerals of the orthosilicate group. *Hydrometallurgy* **2014**, *150*, 68–82. [CrossRef]
47. Dietzen, C.; Harrison, R.; Michelsen-Correa, S. Effectiveness of enhanced mineral weathering as a carbon sequestration tool and alternative to agricultural lime: An incubation experiment. *Int. J. Greenh. Gas Control* **2018**, *74*, 251–258. [CrossRef]
48. Paulo, C.; Power, I.M.; Stubbs, A.R.; Wang, B.; Zeyen, N.; Wilson, S. Evaluating feedstocks for carbon dioxide removal by enhanced rock weathering and CO<sub>2</sub> mineralization. *Appl. Geochem.* **2021**, *129*, 104955. [CrossRef]
49. Daval, D.; Hellmann, R.; Martinez, I.; Gangloff, S.; Guyot, F. Lizardite serpentine dissolution kinetics as a function of pH and temperature, including effects of elevated pCO<sub>2</sub>. *Chem. Geol.* **2013**, *351*, 245–256. [CrossRef]
50. Van Noort, R.; Mørkved, P.; Dundas, S. Acid Neutralization by Mining Waste Dissolution under Conditions Relevant for Agricultural Applications. *Geosciences* **2018**, *8*, 380. [CrossRef]
51. Huijgen, W.J.J.; Witkamp, G.-J.; Comans, R.N.J. Mechanisms of aqueous wollastonite carbonation as a possible CO<sub>2</sub> sequestration process. *Chem. Eng. Sci.* **2006**, *61*, 4242–4251. [CrossRef]
52. Chai, Y.E.; Chalouati, S.; Fantucci, H.; Santos, R.M. Accelerated weathering and carbonation (mild to intensified) of natural Canadian silicates (kimberlite and wollastonite) for CO<sub>2</sub> sequestration. *Crystals* **2021**, *11*, 1584. [CrossRef]
53. Santos, R.M.; Van Audenaerde, A.; Chiang, Y.W.; Iacobescu, R.I.; Knops, P.; Van Gerven, T. Nickel extraction from olivine: Effect of carbonation pre-treatment. *Metals* **2015**, *5*, 1620–1644. [CrossRef]
54. Boampong, L.O.; Hyman, J.D.; Carey, W.J.; Viswanathan, H.S.; Navarre-Sitchler, A. Characterizing the combined impact of nucleation-driven precipitation and secondary passivation on carbon mineralization. *Chem. Geol.* **2024**, *663*, 122256. [CrossRef]
55. Harrison, A.L.; Dipple, G.M.; Power, I.M.; Mayer, K.U. Influence of surface passivation and water content on mineral reactions in unsaturated porous media: Implications for brucite carbonation and CO<sub>2</sub> sequestration. *Geochim. Cosmochim. Acta* **2015**, *148*, 477–495. [CrossRef]
56. Johnson, N.C.; Thomas, B.; Maher, K.; Rosenbauer, R.J.; Bird, D.; Brown, G.E. Olivine dissolution and carbonation under conditions relevant for in situ carbon storage. *Chem. Geol.* **2014**, *373*, 93–105. [CrossRef]
57. Di Lorenzo, F.; Ruiz-Agudo, C.; Ibañez-Velasco, A.; Gil-San Millán, R.; Navarro, J.A.R.; Ruiz-Agudo, E.; Rodríguez-Navarro, C. The carbonation of wollastonite: A model reaction to test natural and biomimetic catalysts for enhanced CO<sub>2</sub> sequestration. *Minerals* **2018**, *8*, 209. [CrossRef]
58. Miller, Q.R.S.; Thompson, C.J.; Loring, J.S.; Windisch, C.F.; Bowden, M.E.; Hoyt, D.W.; Hu, J.Z.; Arey, B.W.; Rosso, K.M.; Schaefer, H.T. Insights into silicate carbonation processes in water-bearing supercritical CO<sub>2</sub> fluids. *Int. J. Greenh. Gas Control* **2013**, *15*, 104–118. [CrossRef]



59. Pastero, L.; Giustetto, R.; Aquilano, D. Calcite passivation by gypsum: The role of the cooperative effect. *CrystEngComm* **2017**, *19*, 3649–3659. [[CrossRef](#)]
60. Poonoosamy, J.; Klinkenberg, M.; Deissmann, G.; Brandt, F.; Bosbach, D.; Mader, U.; Kosakowski, G. Effects of solution supersaturation on barite precipitation in porous media and consequences on permeability: Experiments and modelling. *Geochim. Cosmochim. Acta* **2019**, *270*, 43–60. [[CrossRef](#)]
61. Béarat, H.; McKelvy, M.J.; Chizmeshya, A.V.; Gormley, D.; Nunez, R.; Carpenter, R.W.; Squires, K.; Wolf, G.H. Carbon sequestration via aqueous olivine mineral carbonation: Role of passivating layer formation. *Environ. Sci. Technol.* **2006**, *40*, 4802–4808. [[CrossRef](#)]
62. Kashim, M.Z.; Tsegab, H.; Rahmani, O.; Abu Bakar, Z.A.; Aminpour, S.M. Reaction mechanism of wollastonite in situ mineral carbonation for CO<sub>2</sub> sequestration: Effects of saline conditions, temperature, and pressure. *ACS Omega* **2020**, *5*, 28942–28954. [[CrossRef](#)]
63. Dold, B. Acid rock drainage prediction: A critical review. *J. Geochem. Explor.* **2017**, *172*, 120–132. [[CrossRef](#)]
64. Duan, L.; Hao, J.; Xie, S.; Zhou, Z.; Ye, X. Determining weathering rates of soils in China. *Geoderma* **2002**, *110*, 205–225. [[CrossRef](#)]
65. Cao, X.; Li, Q.; Xu, L.; Tan, Y. A review of in situ carbon mineralization in basalt. *J. Rock Mech. Geotech. Eng.* **2024**, *16*, 1467–1485. [[CrossRef](#)]
66. Akisanmi, P. Classification of clay minerals. In *Mineralogy*; IntechOpen: Rijeka, Croatia, 2022. [[CrossRef](#)]
67. Mahmud, M.S.; Chong, K.P. Effects of Liming on Soil Properties and Its Roles in Increasing the Productivity and Profitability of the Oil Palm Industry in Malaysia. *Agriculture* **2022**, *12*, 322. [[CrossRef](#)]
68. Olego, M.A.; Quiroga, M.J.; Mendaña-Cuervo, C.; Cara-Jiménez, J.; López, R.; Garzón-Jimeno, E. Long-Term Effects of Calcium-Based Liming Materials on Soil Fertility Sustainability and Rye Production as Soil Quality Indicators on a Typic Palexerult. *Processes* **2021**, *9*, 1181. [[CrossRef](#)]
69. Rietra, R.P.J.J.; Hiemstra, T.; van Riemsdijk, W.H. Use of Olivine as a Liming Material in Agriculture to Decrease CO<sub>2</sub> Emissions. ResearchGate. 2010. Available online: <https://www.researchgate.net/publication/341017346> (accessed on 6 September 2024).
70. Baek, S.H.; Kanzaki, Y.; Lora, J.M.; Planavsky, N.; Reinhard, C.T.; Zhang, S. Impact of Climate on the Global Capacity for Enhanced Rock Weathering on Croplands. *Earth's Future* **2023**, *11*, e2023EF003698. [[CrossRef](#)]
71. Mati Carbon. Science—Mati Carbon. 2023. Available online: <https://www.mati.earth/the-science/> (accessed on 6 September 2024).
72. Beerling, D.J.; Kantzas, E.P.; Lomas, M.R.; Wade, P.; Eufrazio, R.M.; Renforth, P.; Sarkar, B.; Andrews, M.G.; James, R.H.; Pearce, C.R.; et al. Potential for large-scale CO<sub>2</sub> removal via enhanced rock weathering with croplands. *Nature* **2020**, *583*, 242–248. [[CrossRef](#)]
73. Aramburu Merlos, F.; Silva, J.V.; Baudron, F.; Hijmans, R.J. Estimating lime requirements for tropical soils: Model comparison and development. *Geoderma* **2023**, *432*, 116421. [[CrossRef](#)]
74. Degryse, F.; Smolders, E.; Parker, D.R. Mechanism of Nickel, Magnesium, and Iron Recovery from Olivine. *Environ. Sci. Technol.* **2009**, *43*, 7423–7428. [[CrossRef](#)]
75. Mi, J.; Gregorich, E.; Xu, S.; McLaughlin, N.; Ma, B.; Liu, J. Effect of Bentonite Amendment on soil hydraulic parameters and millet crop performance in a semiarid region. *Field Crops Res.* **2017**, *212*, 107–114. [[CrossRef](#)]

**Disclaimer/Publisher's Note:** The statements, opinions and data contained in all publications are solely those of the individual author(s) and contributor(s) and not of MDPI and/or the editor(s). MDPI and/or the editor(s) disclaim responsibility for any injury to people or property resulting from any ideas, methods, instructions or products referred to in the content.